of CTDs on *Gag* functions, we next tested the functional interaction between CTDs and *Env*. The *Env* incorporation onto the virion was examined by tripartite-transfection of expression vectors for *Env*, *gag-pol*, and SEC14L1a derivatives into 293T cells, and the VLP was collected by centrifugation. The immunoblotting against gp120 was performed on the cell lysate and the VLP fraction. The cellular *Env* and *Gag* expressions were not detectably affected by any of the SEC14L1a derivatives (Fig. 2F, left panel). The *Env* incorporation onto the VLP was slightly enhanced by FL (157%; Fig. 2F, right panel). In contrast, the VLP produced from CTD1- or CTD2-expressing cells incorporated substantially fewer *Env* than those from GFPf-expressing cells (59% or 54%, respectively; Fig. 2F, right panel). These data were reproducible in independently performed experiments. The densitometric analysis of Western blot image showed that the average ± the standard error of the mean of Env incorporation onto the virion was 129.7 ± 39.9%, 54.8 ± 24.7%, and 25.5 ± 10.3% for FL, CTD1, and CTD2 compared to GFPf, respectively (3–4 independent experiments). The *Env*-mediated cell-to-cell fusion assay indicated that SEC14L1a derivatives did not limit the cell surface targeting and function of *Env* (data not shown). In addition, the *Gag* processing in virion was unaffected by any of the SEC14L1a derivatives (data not shown). Collectively, these data suggest that the HIV-1 replication is inhibited by CTD1 and CTD2 due to the inefficient *Env* incorporation onto the virion. To test this possibility, we infected fresh MT-4 cells with the equal amount of HIV-1 propagated in CTD1- or CTD2-expressing MT-4 cells (1–2 ng $p24^{CA}$), and the viral replication was monitored at 3–4 days post-infection by measuring the $p24^{CA}$ concentration. The infectivity of HIV-1 propagated in CTD1- or CTD2-expressing cells was attenuated to 83.1 ± 17.9% or 82.4 ± 5.5% relative to the virus recovered from GFP-expressing cells, respectively (the average ± the standard error of the mean of 3 independent experiments). Altogether, these data suggest that the inhibition of HIV-1 replication by CTD1 and CTD2 is attributed to the attenuation of viral infectivity by lowering the *Env* incorporation onto the virion.

4. Discussion

In the present study, we provide the first evidence that the C-terminal fragment of SEC14L1a functions as an inhibitor of HIV-1 replication. The advantage of this system is that, since MT-4 cells are stably transduced with a cDNA library, the anti-HIV-1 function of a candidate gene is not due to a perturbed cell physiology. This system has been successful in identifying CD14, CD63, and Brd4-CTD as regulators of HIV-1 replication [1,3,4], and more candidates are being analyzed. Among the candidates, SEC14L1a CTD appeared to be one of the relatively modest inhibitors of HIV-1 replication. However, of note, the SEC14L1a derivatives have not been identified in other genetic screening systems. These facts point that our T cell-based system is sensitive in detecting the modest anti-HIV-1 activity of a gene, and is a unique tool in the pursuit of HIV-1 regulatory factors to complete the HIV-1-host interactome.

SEC14L1a may affect the Golgi-mediated vesicular trafficking since SEC14L1a lowers the cell surface levels of cholinergic transporters [23]. However, we do not have any data to suggest that SEC14L1a and its derivatives affect the cell surface targeting of membrane proteins including CD4, CXCR4 and *Env*. These data suggest that SEC14L1a's effect on cholinergic receptor expression is specific, and that the CTD's ability to inhibit HIV-1 replication is independent from SEC14L1a's regulatory functions on vesicular trafficking. The action point of CTD1 and CTD2 was shown to be the late phase of the viral life cycle. Given that CTD1 and CTD2 did not inhibit the biogenesis and the cell surface targeting of *Gag* and *Env*, the major mechanism of CTD1 and CTD2 to inhibit HIV-1 replication was to reduce the infectivity of HIV-1 by limiting the *Env* incorporation onto the virion. Consistent with this idea, the viral infectivity of virions produced in CTDs-expressing cells was attenuated. Then, how do CTDs block the *Env* incorporation onto the virion? We detected a weak interaction between *Gag* and CTD1 or CTD2 by immuno-coprecipitation analysis. Thus, we speculate that the interaction between *Env* and *Gag* at the plasma membrane is interfered by *Gag*-CTDs interaction, resulting in the reduction of *Env* incorporation onto the virion.

The CTD1 was an inhibitor of HIV-1 replication. While the CTD1 negatively affected the *Env* incorporation onto the virion, it positively affected the HIV-1 production. These observations may be seemingly controversial. However, the SEC14L1a derivatives' effect on HIV-1 replication is a summation of their effects of on each step of the viral life cycle. Therefore, it is conceivable that CTD1 can serve as a negative regulator of HIV-1 replication as well as a positive and negative factor on distinct steps of the viral life cycle. These seemingly controversial findings may be in part due to the cells in which the biological functions of SEC14L1a derivatives were examined. The effect of SEC14L1a derivatives on HIV-1 replication was investigated in MT-4 cells, whereas those on the HIV-1 production and *Env* incorporation onto the virion were examined in 293T cells. Although the basic biological features are largely shared among different cell types, it is possible that the SEC14L1a derivatives may function slightly differently in MT-4 cells from 293T cells given that the intracellular distribution of SEC14L1a derivatives in MT-4 cells was not identical to that in 293T cells (Fig. 1E and 1F).

Elucidating the molecular mechanism underlying CTDs' activity not only provides a hint to understand how the HIV-1 virion actively uptakes *Env* through the *Gag-Env* interaction, but also leads to the development of a novel anti-retroviral drug that lowers the infectivity of the virus by preventing *Env* incorporation onto the virion. This is the strength of our T cell-based assay since CTDs inhibit HIV-1 replication specifically. In the previous study, we proposed that a small portion of Brd4 may serve as a therapeutic molecular target for HIV-1 infection, since the constitutive expression of Brd4-CTD limited HIV-1 replication specifically [3], akin to the SEC14L1a CTDs. However, it remains to be examined whether the SEC14L1a and Brd4 derivatives inhibit HIV-1 replication in primary HIV-1 target cells.

The genome-wide screening has potential caveats, including a cDNA bias and a cell line bias. A cDNA library is not a perfect representation of mRNA expressed in the cells from which the library is constructed. For example, the longer the mRNA, the less efficiently the full-length cDNA is synthesized. In fact, we isolated Brd4-CTD from the PBL cDNA library as a potent inhibitor of HIV-1 replication [3]. However, although Brd4 (approximately 5000 nt mRNA in length) is expressed in MT-4 cells, we were unable to recover Brd4-CTD from the MT-4 cDNA library [3]. This clearly demonstrates the cDNA bias in the genetic screening. A cDNA library derived from non-T cells does not contain genes specifically expressed in T cells. Thus, we have to explore many more cDNA libraries to completely cover the genetic diversity of human cells. The cDNA libraries isolated from long-term non-progressors of HIV-1-seropositive individuals or from elite controllers might be of particular interest, considering that a dominant innate HIV-1 resistance gene, such as CCR5 delta 32, may partly account for the slow progression of AIDS. Similarly, use of a particular cell line and/or virus strain may bias the results. MT-4 cells are positive for HTLV-1, and are able to support robust HIV-1 replication. MT-4 cells do not express CCR5, and are unable to support R5-tropic HIV-1 strains. What if other T cell lines and R5-tropic viral strains are used? What if we assay the same cDNA library in TZM-bl cells? We plan to address these issues in the future studies.

In conclusion, genome-wide genetic screening is a powerful tool for identifying the regulatory factors of HIV-1 replication and innate HIV-1 resistance factors that limit HIV-1 infection and AIDS progression. The HIV-1-host interactome should also reveal poten-

Please cite this article in press as: Urano E, et al. T cell-based functional cDNA library screening identified SEC14-like 1a carboxy-terminal domain as a negative regulator of human immunodeficiency virus replication. Vaccine (2009), doi:10.1016/j.vaccine.2009.07.084

tial therapeutic molecular targets that may be used to develop novel anti-AIDS drugs to tackle the emerging drug resistant viruses. However, the fact that different experimental systems often yield non-overlapping candidates suggests that we have to explore more experimental systems to fully understand the HIV-1-host interactome. Our T cell-based system provides an alternative tool for identifying novel HIV-1 regulatory factors, and should help us understand the HIV-1-host interaction in more detail.

Acknowledgements

This work was supported by the Japan Health Science Foundation, the Japanese Ministry of Health, Labor and Welfare, and the Japanese Ministry of Education, Culture, Sports, Science and Technology.

Conflict of interest: None.

References

[1] Kawano Y, Yoshida T, Hieda K, Aoki J, Miyoshi H, Koyanagi Y. A lentiviral cDNA library employing lambda recombination used to clone an inhibitor of human immunodeficiency virus type 1-induced cell death. J Virol 2004;78(20):11352–9.
[2] Valente ST, Goff SP. Inhibition of HIV-1 gene expression by a fragment of hnRNP U. Mol Cell 2006;23(4):597–605.
[3] Urano E, Kariya Y, Futahashi Y, Ichikawa R, Hamatake M, Fukazawa H, et al. Identification of the P-TEFb complex-interacting domain of Brd4 as an inhibitor of HIV-1 replication by functional cDNA library screening in MT-4 cells. FEBS Lett 2008;582(29):4053–8.
[4] Yoshida T, Kawano Y, Sato K, Ando Y, Aoki J, Miura Y, et al. A CD63 mutant inhibits T-cell tropic human immunodeficiency virus type 1 entry by disrupting CXCR4 trafficking to the plasma membrane. Traffic 2008;9(4):540–58.
[5] Zhou H, Xu M, Huang Q, Gates AT, Zhang XD, Castle JC, et al. Genome-scale RNAi screen for host factors required for HIV replication. Cell Host Microbe 2008;4(5):495–504.
[6] Brass AL, Dykxhoorn DM, Benita Y, Yan N, Engelman A, Xavier RJ, et al. Identification of host proteins required for HIV infection through a functional genomic screen. Science 2008;319(5865):921–6.
[7] Konig R, Zhou Y, Elleder D, Diamond TL, Bonamy GM, Irelan JT, et al. Global analysis of host-pathogen interactions that regulate early-stage HIV-1 replication. Cell 2008;135(1):49–60.
[8] Valente ST, Gilmartin GM, Mott C, Falkard B, Goff SP. Inhibition of HIV-1 replication by eIF3f. Proc Natl Acad Sci USA 2009;106(11):4071–8.
[9] Aiken C. Pseudotyping human immunodeficiency virus type 1 (HIV-1) by the glycoprotein of vesicular stomatitis virus targets HIV-1 entry to an endocytic pathway and suppresses both the requirement for Nef and the sensitivity to cyclosporin A. J Virol 1997;71(8):5871–7.
[10] Akari H, Uchiyama T, Fukumori T, Iida S, Koyama AH, Adachi A. Pseudotyping human immunodeficiency virus type 1 by vesicular stomatitis virus G protein does not reduce the cell-dependent requirement of vif for optimal infectivity: functional difference between Vif and Nef. J Gen Virol 1999;80(Pt 11):2945–9.
[11] Chazal N, Singer G, Aiken C, Hammarskjold ML, Rekosh D. Human immunodeficiency virus type 1 particles pseudotyped with envelope proteins that fuse at low pH no longer require Nef for optimal infectivity. J Virol 2001;75(8):4014–8.
[12] Komano J, Miyauchi K, Matsuda Z, Yamamoto N. Inhibiting the Arp2/3 complex limits infection of both intracellular mature vaccinia virus and primate lentiviruses. Mol Biol Cell 2004;15(12):5197–207.
[13] Goff SP. Knockdown screens to knockout HIV-1. Cell 2008;135(3):417–20.
[14] Urano E, Aoki T, Futahashi Y, Murakami T, Morikawa Y, Yamamoto N, et al. Substitution of the myristoylation signal of human immunodeficiency virus type 1 Pr55Gag with the phospholipase C-delta1 pleckstrin homology domain results in infectious pseudovirion production. J Gen Virol 2008;89(Pt 12):3144–9.
[15] Futahashi Y, Komano J, Urano E, Aoki T, Hamatake M, Miyauchi K, et al. Separate elements are required for ligand-dependent and–independent internalization of metastatic potentiator CXCR4. Cancer Sci 2007;98(3):373–9.
[16] Zufferey R, Dull T, Mandel RJ, Bukovsky A, Quiroz D, Naldini L, et al. Self-inactivating lentivirus vector for safe and efficient in vivo gene delivery. J Virol 1998;72(12):9873–80.
[17] Shimizu S, Urano E, Futahashi Y, Miyauchi K, Isogai M, Matsuda Z, et al. Inhibiting lentiviral replication by HEXIM1, a cellular negative regulator of the CDK9/cyclin T complex. AIDS 2007;21(5):575–82.
[18] Chinen K, Takahashi E, Nakamura Y. Isolation and mapping of a human gene (SEC14L), partially homologous to yeast SEC14, that contains a variable number of tandem repeats (VNTR) site in its 3′ untranslated region. Cytogenet Cell Genet 1996;73(3):218–23.
[19] Howe AG, McMaster CR. Regulation of phosphatidylcholine homeostasis by Sec14. Can J Physiol Pharmacol 2006;84(1):29–38.
[20] Saito K, Tautz L, Mustelin T. The lipid-binding SEC14 domain. Biochim Biophys Acta 2007;1771(6):719–26.
[21] Mousley CJ, Tyeryar KR, Vincent-Pope P, Bankaitis VA. The Sec14-superfamily and the regulatory interface between phospholipid metabolism and membrane trafficking. Biochim Biophys Acta 2007;1771(6):727–36.
[22] Anantharaman V, Aravind L. The GOLD domain, a novel protein module involved in Golgi function and secretion. Genome Biol 2002;3(5), research0023.0021-0023.0027.
[23] Ribeiro FM, Ferreira LT, Marion S, Fontes S, Gomez M, Ferguson SS, et al. SEC14-like protein 1 interacts with cholinergic transporters. Neurochem Int 2007;50(2):356–64.

Please cite this article in press as: Urano E, et al. T cell-based functional cDNA library screening identified SEC14-like 1a carboxy-terminal domain as a negative regulator of human immunodeficiency virus replication. Vaccine (2009), doi:10.1016/j.vaccine.2009.07.084

Dominant-negative derivative of EBNA1 represses EBNA1-mediated transforming gene expression during the acute phase of Epstein–Barr virus infection independent of rapid loss of viral genome

Yumi Kariya,[1,2] Makiko Hamatake,[1] Emiko Urano,[1] Hironori Yoshiyama,[3] Norio Shimizu[2] and Jun Komano[1,4]

[1]AIDS Research Center, National Institute of Infectious Diseases, Tokyo; [2]Department of Virology, Division of Medical Science, Medical Research Institute, Tokyo Medical and Dental University, Tokyo; [3]Research Center for Infection-associated Cancer, Institute for Genetic Medicine, Hokkaido University, Sapporo, Japan

(Received November 1, 2009/Revised November 30, 2009/Accepted December 6, 2009)

The oncogenic human herpes virus, the Epstein–Barr virus (EBV), expresses EBNA1 in almost all forms of viral latency. EBNA1 plays a major role in the maintenance of the viral genome and in the transactivation of viral transforming genes, including EBNA2 and latent membrane protein (LMP-1). However, it is unknown whether inhibition of EBNA1 from the onset of EBV infection disrupts the establishment of EBV's latency and transactivation of the viral oncogenes. To address this, we measured EBV infection kinetics in the B cell lines BALL-1 and BJAB, which stably express a dominant-negative EBNA1 (dnE1) fused to green fluorescent protein (GFP). The EBV genome was surprisingly unstable 1 week post-infection: the average loss rate of EBV DNA from GFP- and GFP-dnE1-expressing cells was 53.4% and 41.0% per cell generation, respectively, which was substantially higher than that of an 'established' *oriP* replicon (2–4%). GFP-dnE1 did not accelerate loss of the EBV genome, suggesting that EBNA1-dependent licensing of the EBV genome occurs infrequently during the acute phase of EBV infection. In the subacute phase, establishment of EBV latency was completely blocked in GFP-dnE1-expressing cells. In contrast, C/W promoter-driven transcription was strongly restricted in GFP-dnE1-expressing cells at 2 days post-infection. These data suggest that inhibition of EBNA1 from the onset of EBV infection is effective in blocking the positive feedback loop in the transactivation of viral transforming genes, and in eradicating the EBV genome during the subacute phase. Our results suggest that gene transduction of GFP-dnE1 could be a promising therapeutic and prophylactic approach toward EBV-associated malignancies. (*Cancer Sci* 2010)

The Epstein–Barr virus (EBV) is a risk factor in several malignant diseases including Burkitt's lymphoma and nasopharyngeal carcinoma.[1–4] The opportunistic B-cell lymphoma is becoming the major cause of death in AIDS patients in an era of highly active antiretroviral therapy (HAART), and EBV is associated with a significant portion of AIDS lymphoma cases.[5,6] Neither an EBV vaccine, nor specific antiviral agents against EBV are available; thus attention should be paid to the development of therapeutic agents against EBV.

EBV-encoded genes including EBNA1, EBNA2, and latent membrane protein (LMP-1) are potential molecular targets for the treatment of EBV-associated lymphomas because they play central roles in the process of malignant transformation.[7] We are interested in EBNA1 since it contributes to EBV oncogenesis in two ways: it supports the maintenance of the EBV genome in *cis* and enhances expression of viral oncogenes, including EBNA2 and LMP-1, in *trans*.[7–9] EBNA1 exerts its biological functions by binding to its cognate binding sites within the family of repeats (FR) and the dyad symmetry element (DS) located within the origin of replication (oriP) of EBV DNA. EBNA1 interacts with FR to enhance transcription from the viral C/W promoters (C/Wp) and to partition EBV DNA to daughter cells; and with DS to initiate DNA replication.[7–9]

Maintenance of the oriP replicon is stable once EBV latency has been established. The loss rate of established oriP plasmids is estimated at 2–4% per cell generation.[10,11] Interestingly, the loss rate of the oriP replicon is significantly higher in cells transiently transduced with oriP plasmids (>25% per cell generation) than in established cells.[12] In primary B cells, EBV DNA is lost rapidly within 2 days post-infection (~98.9%).[13] However, the loss rate of the EBV genome during a week post-infection in B cells remains to be quantified.

Upon EBV infection, the first viral genes expressed are the transactivators EBNA2 and EBNA-LP transcribed from Wp several hours after infection.[7] EBNA2 binds to the EBNA2-responsive elements and, in cooperation with EBNA-LP, enhances transcription from Cp, which leads to expression of all EBNA proteins, including EBNA1. EBNA1 binding to oriP activates C/Wp to boost viral latent gene expression, including the EBNAs and LMP-1. The viral gene transactivation positive feedback loop is established within a few days post-infection, and EBNA1 is one of the key factors that sustain this feedback loop during the acute phase of EBV infection.[14] In parallel, EBNA1 contributes to the establishment of the EBV genome as a licensed replicon. It may be possible to stop EBV infection by breaking the chain of EBNA1-dependent events and thus the EBV-mediated malignant transformation of infected cells. Previous studies have assessed the therapeutic potential of a dominant-negative derivative of EBNA1 (dnE1) in cells in which EBV latency was already established.[15,16] In this study, we critically assessed whether inhibition of EBNA1 limits the early stage of EBV infection in B cells. We provide evidence that expression of dnE1 strongly blocks the expression of virus-encoded oncogenes in acutely infected cells without accelerating EBV genome loss, and disrupts EBV latency in the subacute phase of EBV infection.

Materials and Methods

Cells. The 293T, EBV-negative Burkitt lymphoma cell line BJAB, EBV-positive Burkitt lymphoma cell line Daudi, EBV-transformed healthy donor-derived B lymphoblastoid cell line (B-LCL), and B acute lymphoblastic leukemia cell line BALL-1

[4]To whom correspondence should be addressed.
E-mail: ajkomano@nih.go.jp

doi: 10.1111/j.1349-7006.2009.01474.x

cells (kindly provided by Dr. Yokota, National Institute of Infectious Diseases, Tokyo, Japan) were maintained in RPMI-1640 medium (Sigma, St. Louis, MA, USA) supplemented with 10% fetal bovine serum (Japan Bioserum, Tokyo, Japan), 50 U/mL penicillin, 50 μg/mL streptomycin (Invitrogen, Tokyo, Japan), and incubated at 37°C in a humidified 5% CO_2 atmosphere.

Plasmids. The following primers were used to amplify dnE1 from p1160[17] by PCR: 5′-ACCGGTCTCGAGCAATTGCCA-CCATGCGGGGTCAGGGTGATGGAGG-3′ and 5′-GGATC-CTCGAGCGGCCGCTCACTCCTGCCCTTCCTCACC-3′. The GFP-dnE1 expression vector (pGD) was constructed by cloning the MfeI-XhoI fragment of the PCR product into the BglII-SalI sites of pEGFP-C1 (Clontech, Palo Alto, CA, USA). The MfeI and BglII sites were blunted with T7 RNA polymerase. The AgeI-BamHI fragment from pGD was cloned into the corresponding restriction sites of pCMMP eGFP[15,18] to generate pCMMP GFP-dnE1. The EBNA1 expression vector p1553, the FR-tk-luciferase reporter p985, and pLuciferase (pCMV-luc) have been described previously.[17–20]

Luciferase assay. The 293T cells, grown in 48-well plates, were co-transfected with the indicated plasmids using Lipofectamine 2000 according to the manufacturer's protocol (Invitrogen, Tokyo, Japan). Cells were replated in 96-well plates in triplicate at 2 h post-transfection. Luciferase activity was measured 48 h after transfection using the Steady-Glo Kit (Promega, Madison, WI, USA).

Murine leukemia virus (MLV) vector infection and cell sorting. MLV vectors were produced as described previously.[18] B cells (1×10^7 cells) were incubated with 2 mL of MLV preparation overnight at 4°C with continuous agitation. GFP-positive cells were collected using a FACS sorter (FACS Vantage; Becton Dickinson, San Jose, CA, USA) at 11 days post-infection.

Western blotting. Western blotting was performed as described previously.[21,22] The following reagents were used: anti-GFP (MsX Green Fluorescent Protein; Chemicon, Temecula, CA, USA) and Envision$^+$ Dual Link System-HRP (Dako, Glostrup, Denmark).

EBV infection and nucleic acid extraction. The EBV B95-8 strain was a generous gift from Dr Fujiwara's group at the National Research Institute for Child and Development (Tokyo, Japan). B cells (1×10^7 cells) were incubated with 100 μL of B95-8 EBV for 1 h at 37°C, and genomic DNA was extracted from half of the infected cells soon after infection (QIAamp DNA Mini Kit; Qiagen, Tokyo, Japan). At 15 h post-infection, half of the cells were washed once with PBS and incubated for 5 min in lysis buffer (10 mM Tris-HCl [pH7.4], 10 mM NaCl, 3 mM $MgCl_2$, and 0.5% NP-40). The nuclear fraction was collected by centrifugation for 5 min at 20.6 K × *g* (Kubota 3740; Kubota, Tokyo, Japan), and high molecular weight DNA was extracted (nuclear DNA). At 2 days post-infection and at later time points, high molecular weight DNA, or total RNA (PureLink Total RNA Blood Purification Kit; Invitrogen) was extracted from 1×10^6 or 3×10^6 cells, respectively, according to the manufacturer's protocol. After EBV infection, 10 μM aciclovir (Kayaku, Tokyo, Japan) was added to the culture medium. The production and infection of the recombinant EBV Akata strain carrying GFP and neomycin resistant genes has been described previously.[23] At 2 days post-infection, cells were plated at a density of 1×10^4 cells per well in a flat-bottomed 96-well plate, and cultured in a medium containing 1 mg/mL G418. The efficiency of EBV latency establishment was evaluated as percentage of wells positive for the emergence of G418-resistant cells at 2 to 3 weeks post-G418 selection.

Quantitative real-time PCR. Real-time PCR was performed as described previously; serial dilutions of positive controls were used as standards.[21] Amplifications were performed using the QuantiTect SYBR Green RT-PCR/PCR Kit (Qiagen), and the following primers: BamHI W repeat, 5′-GCCAGAGG-TAAGTGGACTTT-3′ and 5′-AGAAGCATGTATACTAAGC-CTCCC-3′; cyclophilin A (CYPA), 5′-CACCGCCACCATG-GTCAACCCCA-3′ and 5′-CCCGGGCCTCGAGCTTTCGAG-TTGTCCACAGTCAGCAATGG-3′; C/Wp, 5′-CCCTCGGA-CAGCTCCTAAG-3′ and 5′-CTTCACTTCGGTCTCCCCTA-3′; EBER1, 5′-AAAACATGCGGACCACCAGC-3′ and 5′-AG-GACCTACGCTGCCCTAGA-3′. The β-globin primers were described previously.[21] Following PCR amplification, the amplicons were separated in a 2% agarose gel, stained with ethidium bromide, and imaged with a Typhoon scanner (GE Healthcare Bio-Sciences; Piscataway, NJ, USA).

Results

Construction and functional verification of dnE1 fused to GFP. The carboxy half of EBNA1 serves as a functional dominant-negative inhibitor of EBNA1 that restricts the replication and maintenance of oriP plasmids as well as the EBNA1-dependent enhancement of transcription.[17,24] We used a dnE1 mutant encompassing amino acids 377 to 391 (the nuclear localization signal, NLS) and 451 to 641 (the DNA binding and dimerization domain) of EBNA1 (Fig. 1A).[17] To visualize the intracellular distribution of dnE1, we constructed the retroviral expression vector encoding GFP-dnE1. The expression of GFP-dnE1 was verified in transiently transfected 293T cells and stably transduced B cell lines using an MLV vector. To verify the function of GFP-dnE1, we conducted a reporter assay using a plasmid encoding the FR-tk-luciferase cassette. EBNA1 enhances expression of FR-tk-luciferase by binding to FR. If the GFP-dnE1 construct retains dnE1 function, co-expressing EBNA1 and GFP-dnE1 should reduce reporter activity. Luciferase activity was increased significantly upon EBNA1 expression by approximately 5.3-fold, consistent with previous findings (Fig. 1B, $P < 0.05$, two-tailed Student's *t*-test).[17] When GFP-dnE1 was co-expressed, the luciferase activity was decreased. The decrease in luciferase activity was proportional to the increase in GFP-dnE1 expression vector (Fig. 1B, maximum reduction: 22.3%, $P < 0.05$, two-tailed Student's *t*-test). This effect was not observed with GFP alone. In addition, CMV promoter-driven luciferase expression was unaffected by EBNA1, GFP-dnE1, and GFP, suggesting that the reduction in luciferase activity with GFP-dnE1 in the EBNA1/FR-tk-luciferase system is specific. These data indicate that GFP-dnE1 functions as an inhibitor of EBNA1.

Establishment of B cells constitutively expressing GFP-dnE1. To investigate the potential effect of GFP-dnE1 on EBV infection in B cells, we established BALL-1 and BJAB cells, which constitutively express GFP-dnE1, using an MLV vector. GFP was used as a control throughout this study. The distribution of GFP-dnE1 was examined by confocal microscopy, which revealed an even distribution of GFP throughout the cell. In contrast, the majority of GFP-dnE1was localized to the nucleus due to the presence of the NLS (Fig. 2A). Similar observations were made in BJAB and 293T cells (data not shown). We sorted the GFP- or GFP-dnE-expressing cells using a FACS sorter. To test the dose-dependent effect, we collected BALL-1 cell populations bearing high or low levels of GFP fluorescence, denoted as Hi and Lo, respectively. The expression of GFP and GFP-dnE1 was verified by Western blotting, which confirmed that GFP and GFP-dnE1 Hi cells had higher intensity signals than the GFP and GFP-dnE1 Lo cells (Fig. 2B). The rate of cell proliferation and the morphology of GFP-dnE1 cells were indistinguishable from those of GFP cells (Fig. 2A and data not shown).

Effect of GFP-dnE1 on the nuclear translocation of EBV DNA during the acute phase of EBV infection. To assess whether GFP-dnE1 could restrict the nuclear targeting of the EBV

doi: 10.1111/j.1349-7006.2009.01474.x

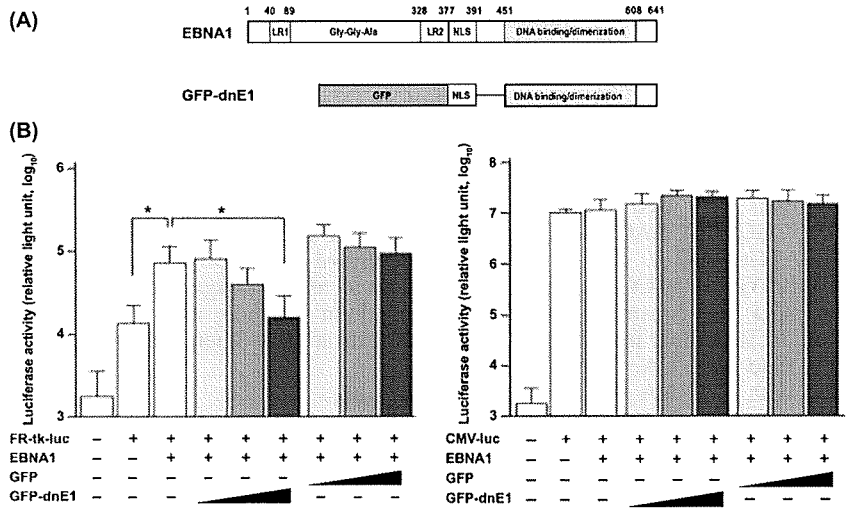

Fig. 1. Construction and functional characterization of a dominant-negative EBNA1 mutant (dnE1) fused to green fluorescent protein (GFP). (A) Structure of the EBNA1 protein and dnE1 used in this study. The linking regions (LR1 and LR2), the Gly-Gly-Ala repeat, the nuclear localization signal (NLS), and the DNA binding and dimerization domain are shown. GFP-dnE1 encodes the NLS and DNA binding and dimerization domain of EBNA1 fused to the C-terminus of GFP. (B) Repression of EBNA1-dependent transcriptional activation by GFP-dnE1. We transfected 293T cells in 48-well plates with 200 ng of FR-tk-luc or CMV-luc reporter, and 500 ng of EBNA1 expression vector, along with increasing amounts of GFP or GFP-dnE1 expression vector (20, 100, and 500 ng, respectively). $*P < 0.05$, two-tailed Student's *t*-test.

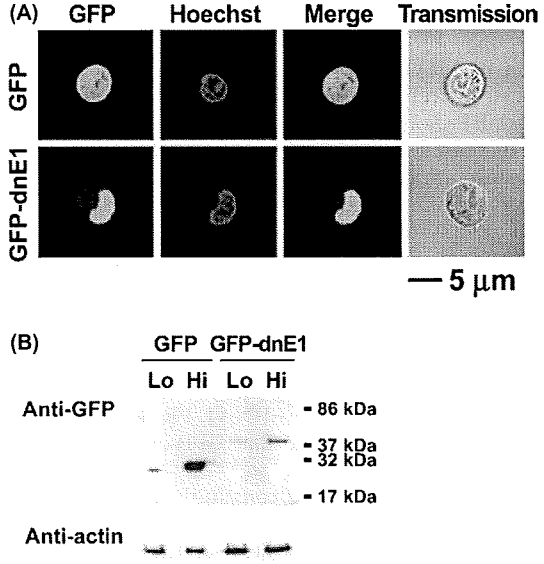

Fig. 2. Verification of stable green fluorescent protein (GFP)-dominant-negative EBNA1 (dnE1) expression in BALL-1 cells. (A) Distribution of GFP and GFP-dnE1 in BALL-1 cells was examined by confocal microscopy. Cells were imaged unfixed using a confocal microscope META 510 (Carl Zeiss, Tokyo, Japan). The green signal represents GFP fluorescence, and blue represents the Hoechst-stained nucleus. The bar represents 5 μm; magnification, ×630. (B) GFP or GFP-dnE1 expression in stably transduced BALL-1 cells was examined by Western blot analysis using an anti-GFP antibody. Protein lysates from 5×10^5 cells were loaded for each sample, except GFP Hi cells (5×10^4). The molecular weight marker is shown on the right.

genome after infection, we measured the amount of EBV DNA recovered from cells immediately after infection (representing the amount of EBV attached to cells) and the amount of EBV DNA that had migrated into the nucleus at 1 day post-infection. We isolated the nuclear fraction to exclude EBV DNA that failed to enter the nucleus. The number of EBV DNA molecules per cell was estimated by real-time PCR, which targeted the BamHI W repeat, in 10 ng of genomic DNA. We estimated the number of EBV DNA per cell given that a single cell contains approximately 10 pg of genomic DNA, and an EBV DNA has 10 copies of BamHI W repeats on average. The nuclear targeting efficiencies of EBV DNA were as follows: BALL-1 GFP cells, 43.3–108.6%; GFP-dnE1 cells, 46.9–65.6%; BJAB GFP cells, 37.4%; GFP-dnE1 cells, 35.0% (Table 1). These data suggested that the effect of GFP-dnE1 on the nuclear targeting of EBV DNA should be assessed more sensitively in BALL-1 and BJAB cell systems than in primary B cells because the nuclear targeting efficiency of EBV DNA in primary B cells is extremely inefficient (~1.1%).[13] In our experimental systems, the nuclear targeting efficiencies of EBV DNA in GFP-dnE1-expressing cells were similar to those in GFP-expressing cells. In addition, the dose-dependency of GFP-dnE1 was not observed in BALL-1 cells (Table 1). These data suggest that the nuclear targeting efficiency of EBV DNA was not restricted by the presence of GFP-dnE1 in B cells upon EBV infection.

Effect of GFP-dnE1 on the rate of loss of EBV DNA during the acute phase of EBV infection. To examine the effect of GFP-dnE1 on the rate of loss (ROL) of EBV DNA during the acute phase of viral infection, we monitored the EBV DNA copy number from day 2 to day 5 or day 6 post-infection, by real-time PCR, which detects the viral genome in both linear and circular configurations (Table 1). The ROL was estimated as the percentage reduction of EBV DNA per cell generation, considering that the cell doubling time is 24 h, and the kinetics of viral genome loss follows an exponential decay. The ROL in GFP-dnE1-expressing cells (19.2–85.9% per cell generation) was similar to GFP-expressing cells (20.5–79.4% per cell generation) in both BALL-1 and BJAB cells. In addition, there was no detectable dose-dependent effect of GFP-dnE1 in BALL-1 cells (Table 1 and Fig. 3). The averages ± SEs of ROL in GFP- and GFP-dnE1-expressing cells from six independent measurements in BALL-1 cells were 37.7 ± 10.7% and 25.7 ± 6.5% per cell generation, respectively (data not shown), which was substantially higher than the rate of loss of an established oriP replicon (2–4%).[10,11] These results reflect the precipitous loss of oriP plas-

Table 1. The kinetics of EBV DNA in the acute phase of EBV infection

Cell	Copy number of EBV DNA per cell at the indicated day†				Nuclear transport (%‡)	Rate of loss of EBV DNA (% per cell generation§)
Expt 1						
BALL-1	Day 0	Day 1	Day 2	Day 5		
GFP Hi	20.38	11.92	3.57	0.01¶	58.5	85.9
GFP Lo	17.26	11.68	3.21	0.56	67.7	44.1
GFP-dnE1 Hi	23.02	10.79	3.30	0.30	46.9	54.9
GFP-dnE1 Lo	18.83	12.36	1.46	0.53	65.6	28.7
BJAB	Day 0	Day 1	Day 2	Day 5		
GFP	155.1	58.8	5.38	0.06	37.4	77.7
GFP-dnE1	64.6	37.4	5.69	0.05	58.0	79.4
Expt 2						
BALL-1	Day 0	Day 1	Day 2	Day 6		
GFP Hi	16.33	17.73	11.10	4.74	108.6	19.2
GFP Lo	17.35	7.51	8.75	1.13	43.3	40.1
GFP-dnE1 Hi	18.46	8.71	8.95	3.38	47.2	21.6
GFP-dnE1 Lo	14.14	7.05	6.97	2.79	49.9	20.5

†Nuclear DNA was used for day 1 data. ‡Estimated from day 0 and day 1 data. §Estimated from day 2 and day 5 or day 6 data with the exponential decay. ¶Below the limit of detection. dnE1, dominant-negative EBNA1; EBV, Epstein–Barr virus; GFP, green fluorescent protein.

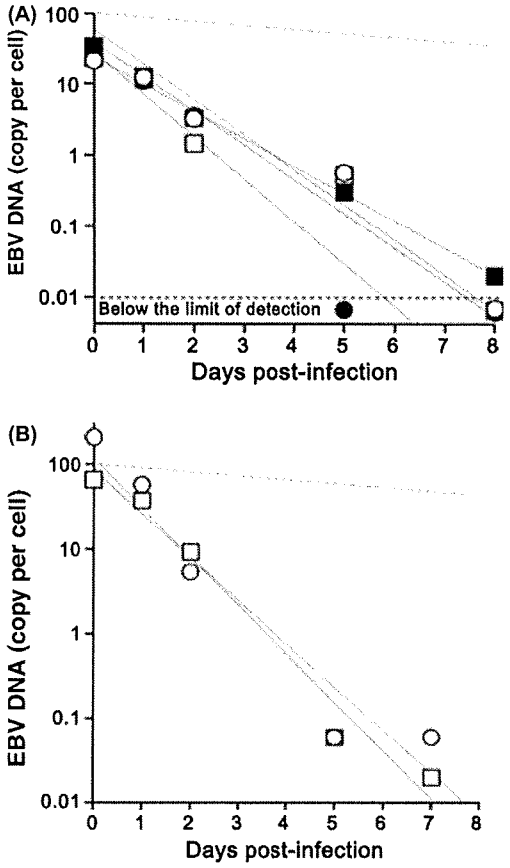

Fig. 3. Kinetics of Epstein–Barr virus (EBV) DNA loss during the acute phase of EBV infection. (A) Representative data from BALL-1 cells (Expt. 1 in Table 1) is shown. The filled squares, open squares, filled circles, and open circles represent GFP Hi, GFP Lo, GFP-dnE1 Hi, and GFP-dnE1 Lo, respectively. The limit of detection was below 0.01 (dashed line). The gray lines represent an approximation to the exponential decay. The dashed gray line represents the 4% rate of loss per cell generation. (B) Representative data from BJAB cells shown in Table 1. The circles and squares represent GFP and GFP-dnE1, respectively. Please see Table 1 for the detailed analysis.

mids (26–37%) in transiently transfected non-B cells.[12] The data suggest that GFP-dnE1 is unable to accelerate the ROL in the acute phase of EBV infection in B cells, presumably because the EBV genome is not established as an EBNA1-dependent stable licensed replicon. It should be noted that this is the first time that quantitative ROL data has been obtained by introducing the oriP replicon into B cells via EBV infection, which is an approach that does not confer any selective advantage on the infected cells.

Effect of GFP-dnE1 on efficiency of establishment of EBV latency. Cells infected with recombinant EBV, carrying the neomycin resistance gene, were seeded at 5×10^3 cells per well into a 96-well plate, and the efficiency of the establishment of EBV latency was assessed as the percentage of wells positive for the emergence of G418-resistant cells. G418-resistant cells appeared in BJAB, Daudi, parental BALL-1, and BALL-1 GFP cells at 56–100% efficiencies. In sharp contrast, G418-resistant cells were absent from GFP-dnE1-expressing BALL-1 cells (Table 2). These data clearly suggest that, although the ROL during the acute phase of EBV infection was not enhanced by GFP-dnE1, GFP-dnE1 was able to block the establishment of EBV latency completely during the subacute phase of EBV infection.

Effect of GFP-dnE1 on EBV-encoded latent gene expression. EBV gene expression was tested at 2 days post-infection by quantitative RT-PCR. We focused on the C/Wp activity because it expresses key viral transactivators including EBNA1, -2, -3s, and -LP to boost viral transforming gene expression. We detected C/Wp-driven transcripts in GFP Hi BALL-1 cells as expected. Conversely, C/Wp-driven transcripts were undetectable in GFP-dnE1 Hi and Lo BALL-1 cells, although these cells retained similar EBV DNA levels to GFP-expressing cells (Fig. 4 and Table 3). The Cp-driven transcript was under the limit of detection by RT-PCR, suggesting that the Wp is predominantly activated at the early phase of EBV infection consistent with previous findings.[7] Inhibition of viral gene transcription was not observed in the RNA polymerase III-driven transcript EBER1,[25] and cyclophilin A mRNA levels were similar between GFP- and GFP-dnE1-expressing cells (Fig. 4 and Table 3). This indicates that the effect of GFP-dnE1 on C/Wp activity is specific, and uncovers an active role of EBNA1 in supporting transactiva-

doi: 10.1111/j.1349-7006.2009.01474.x

Table 2. The establishment efficiency of EBV latency

Cell	Emergence of G418-resistant cells†	
BJAB	100%	(6/6)
Daudi	100%	(10/10)
BALL-1		
Parental	56%	(5/9)
GFP Hi	67%	(2/3)
GFP-dnE1 Hi	0%	(0/6)
GFP-dnE1 Lo	0%	(0/6)

†Percentage of wells positive for G418-resistant cells over the number of tested wells from 96-well plates indicated in the bracket. Shown are the sum of two independent experiments. dnE1, dominant-negative EBNA1; EBV, Epstein–Barr virus; GFP, green fluorescent protein.

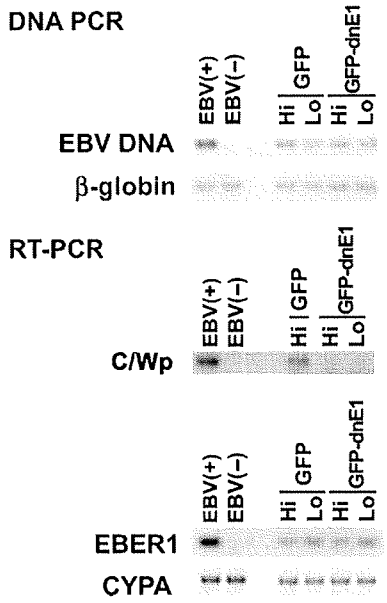

Fig. 4. PCR-based analysis of Epstein–Barr virus (EBV) gene expression. The effect of green fluorescent protein (GFP)-dominant-negative EBNA1 (dnE1) on the loss of EBV DNA (DNA PCR, upper panels) and transcription of the C/W promoter-driven transcript (C/Wp), EBER1, and cyclophilin A (CYPA; RT-PCR, lower panels) in BALL-1 cells at 2 days post-infection were examined. EBV-transformed B-lymphoblastoid cell line (B-LCL) and BJAB cells, denoted as EBV(+) and EBV(−), were used as positive and negative controls for viral DNA and RNA shown, respectively. β-Globin and CYPA were used as controls.

Table 3. Quantification of EBV transcripts in BALL-1 cells by real-time PCR at 2 days post-infection

BALL-1 cells		W1/2 exon (copies†)	EBER1 (copies‡)	CYPA (copies‡)
GFP	Hi	2.2	2.8×10^2	1.4×10^6
	Lo	NT§	0.8×10^2	1.0×10^6
GFP-dnE1	Hi	BLD¶	3.3×10^2	1.3×10^6
	Lo	BLD¶	1.2×10^2	1.5×10^6

†Copies per 13–14 ng total cellular RNA. ‡Copies per 200 ng total cellular RNA. §Not tested. ¶Below the limit of detection. CYPA, cyclophilin A; dnE1, dominant-negative EBNA1; EBV, Epstein–Barr virus; GFP, green fluorescent protein.

tion from C/Wp. Taken together, these results show that inhibition of EBNA1 functions strongly restricts EBV-encoded transforming gene expression and, although there is no detectable effect on the ROL of EBV DNA at the acute phase of viral infection, it blocks the establishment of EBV latency during the subacute phase.

Discussion

This is the first report describing the effect of EBNA1 inhibition from the onset of EBV infection in B cells. Unexpectedly, the dnE1 was unable to accelerate the ROL during the acute phase of EBV infection since dnE1 enhanced the loss of the oriP plasmid in the transient transfection assays.[10,11] In the subacute phase of EBV infection, the establishment of EBV latency was potently blocked by dnE1. In addition, we observed a strong repressive effect of dnE1 on the EBNA1-dependent enhancement of viral gene transcription from C/Wp during the early phase of EBV infection, similar to the transient transfection assays.[17] These data suggest that viral oncogene expression depends heavily on EBNA1 during the acute phase of viral infection, and that EBNA1 contributes little to EBV genome maintenance during this period. The results emphasize that an EBNA1 inhibitor should serve as an attenuator of viral oncogene expression since activation of C/Wp is the 'root' event of the positive feedback loop involved in the transactivation of viral transforming gene expression. In this regard, the EBNA1 inhibition approach could be superior to LMP-1 or EBNA2 inhibition.

If EBNA1 binding to oriP is essential for both the enhancement of viral gene transcription and for genome maintenance, what mechanism prevents dnE1 from affecting the ROL during the acute phase of EBV infection? It is likely that maintenance of the oriP replicon immediately after its introduction into cells is less efficient than in cells harboring an 'established' oriP replicon as an autonomously replicating plasmid. The ROL of an established oriP replicon is 2–4% per cell generation.[10,11] In contrast, our data from the EBV/B cell-based assay gave an average ROL of 26–38% during the week post-infection (acute phase of EBV infection). In agreement with our findings, it is reported that a transiently transduced oriP replicon is lost from cells at 26–37% per cell generation 1–2 weeks post-plasmid transduction.[12] These data indicate that maintenance of the oriP replicon is largely EBNA1-independent immediately after its introduction into cells, regardless of whether the route of introduction is by transfection or EBV infection. In other words, the establishment of EBV latency should be a rare epigenetic event. The data also suggest that the artificial minichromosome approach may be relevant in understanding EBV genome behavior.[12]

Our study suggests that gene therapy using GFP-dnE1 is an attractive approach, not only for therapeutics, but also for prophylactic interventions of EBV-associated malignancies. For example, in peripheral blood stem cell transplantation (PBSCT), GFP-dnE1 transduction into $CD34^+$ cells should protect the differentiated B cells from EBV infection, thus preventing the genesis of EBV-associated B cell lymphomas. We will attempt to prove this hypothesis using a small animal model in future studies.[26] Additionally, EBNA1 is a potential molecular target for developing a small molecular-weight EBV inhibitor as mentioned previously.[14,15] The advantages of EBNA1-inhibitor development are that the biological assay system is already established and the X-ray crystal structure of the DNA-bound EBNA1 DNA binding and dimerization domain is known, which means that computer-aided drug design technology can be immediately applied. Although EBV is associated with various malignancies, preventive and therapeutic measures against EBV infection have not been developed. We believe that an anti-EBV agent, such as an EBNA1 inhibitor, would have an enormous impact in the medical field due to the substantial number of patients with EBV-associated malignancies.

Acknowledgments

We thank Drs Kenichi Imadome and Shigeyoshi Fujiwara for reagents. We also thank Dr Bill Sugden for critically reading the manuscript. This work was supported by the Japan Health Science Foundation, the Ministry of Health, Labor and Welfare of Japan, and the Ministry of Education, Culture, Sports, Science and Technology of Japan.

Disclosure Statement

The authors have no conflict of interest.

References

1 Thompson MP, Kurzrock R. Epstein–Barr virus and cancer. *Clin Cancer Res* 2004; **10**: 803–21.
2 Rickinson AB, Kieff E. Epstin–Barr virus. In: Knipe DM, Howley PM, eds. *Fields Virology*, 5th edn, vol. 2. Philadelphia: Lippincott Williams & Wilkins, 2007; 2655–700.
3 Klein E, Kis LL, Klein G. Epstein–Barr virus infection in humans: from harmless to life endangering virus-lymphocyte interactions. *Oncogene* 2007; **26**: 1297–305.
4 Snow AL, Martinez OM. Epstein–Barr virus: evasive maneuvers in the development of PTLD. *Am J Transplant* 2007; **7**: 271–7.
5 Besson C, Goubar A, Gabarre J *et al.* Changes in AIDS-related lymphoma since the era of highly active antiretroviral therapy. *Blood* 2001; **98**: 2339–44.
6 Carbone A, Cesarman E, Spina M, Gloghini A, Schulz TF. HIV-associated lymphomas and gamma-herpesviruses. *Blood* 2009; **113**: 1213–24.
7 Kieff E, Rickinson AB. Epstin–Barr virus and its replication. In: Knipe DM, Howley PM, eds. *Fields Virology*, 5th edn, vol. 2. Philadelphia: Lippincott Williams & Wilkins, 2007; 2603–54.
8 Lindner SE, Sugden B. The plasmid replicon of Epstein–Barr virus: mechanistic insights into efficient, licensed, extrachromosomal replication in human cells. *Plasmid* 2007; **58**: 1–12.
9 Wang J, Sugden B. Origins of bidirectional replication of Epstein–Barr virus: models for understanding mammalian origins of DNA synthesis. *J Cell Biochem* 2005; **94**: 247–56.
10 Kirchmaier AL, Sugden B. Plasmid maintenance of derivatives of oriP of Epstein–Barr virus. *J Virol* 1995; **69**: 1280–3.
11 Sugden B, Warren N. Plasmid origin of replication of Epstein–Barr virus, oriP, does not limit replication in cis. *Mol Biol Med* 1988; **5**: 85–94.
12 Leight ER, Sugden B. Establishment of an oriP replicon is dependent upon an infrequent, epigenetic event. *Mol Cell Biol* 2001; **21**: 4149–61.
13 Hurley EA, Thorley-Lawson DA. B cell activation and the establishment of Epstein–Barr virus latency. *J Exp Med* 1988; **168**: 2059–75.
14 Altmann M, Pich D, Ruiss R, Wang J, Sugden B, Hammerschmidt W. Transcriptional activation by EBV nuclear antigen 1 is essential for the expression of EBV's transforming genes. *Proc Natl Acad Sci U S A* 2006; **103**: 14188–93.
15 Kennedy G, Komano J, Sugden B. Epstein–Barr virus provides a survival factor to Burkitt's lymphomas. *Proc Natl Acad Sci U S A* 2003; **100**: 14269–74.
16 Nasimuzzaman M, Kuroda M, Dohno S *et al.* Eradication of Epstein–Barr virus episome and associated inhibition of infected tumor cell growth by adenovirus vector-mediated transduction of dominant-negative EBNA1. *Mol Ther* 2005; **11**: 578–90.
17 Kirchmaier AL, Sugden B. Dominant-negative inhibitors of EBNA-1 of Epstein–Barr virus. *J Virol* 1997; **71**: 1766–75.
18 Komano J, Miyauchi K, Matsuda Z, Yamamoto N. Inhibiting the Arp2/3 complex limits infection of both intracellular mature vaccinia virus and primate lentiviruses. *Mol Biol Cell* 2004; **15**: 5197–207.
19 Aiyar A, Sugden B. Fusions between Epstein–Barr viral nuclear antigen-1 of Epstein–Barr virus and the large T-antigen of simian virus 40 replicate their cognate origins. *J Biol Chem* 1998; **273**: 33073–81.
20 Middleton T, Sugden B. EBNA1 can link the enhancer element to the initiator element of the Epstein–Barr virus plasmid origin of DNA replication. *J Virol* 1992; **66**: 489–95.
21 Urano E, Kariya Y, Futahashi Y *et al.* Identification of the P-TEFb complex-interacting domain of Brd4 as an inhibitor of HIV-1 replication by functional cDNA library screening in MT-4 cells. *FEBS Lett* 2008; **582**: 4053–8.
22 Shimizu S, Urano E, Futahashi Y *et al.* Inhibiting lentiviral replication by HEXIM1, a cellular negative regulator of the CDK9/cyclin T complex. *AIDS* 2007; **21**: 575–82.
23 Kanda T, Yajima M, Ahsan N, Tanaka M, Takada K. Production of high-titer Epstein–Barr virus recombinants derived from Akata cells by using a bacterial artificial chromosome system. *J Virol* 2004; **78**: 7004–15.
24 Mackey D, Sugden B. The linking regions of EBNA1 are essential for its support of replication and transcription. *Mol Cell Biol* 1999; **19**: 3349–59.
25 Howe JG, Shu MD. Epstein–Barr virus small RNA (EBER) genes: unique transcription units that combine RNA polymerase II and III promoter elements. *Cell* 1989; **57**: 825–34.
26 Yajima M, Imadome K, Nakagawa A *et al.* A new humanized mouse model of Epstein–Barr virus infection that reproduces persistent infection, lymphoproliferative disorder, and cell-mediated and humoral immune responses. *J Infect Dis* 2008; **198**: 673–82.

doi: 10.1111/j.1349-7006.2009.01474.x

Journal of Cellular Physiology

Dys-Regulated Activation of a Src Tyroine Kinase Hck at the Golgi Disturbs *N*-Glycosylation of a Cytokine Receptor Fms

RANYA HASSAN,[1] SHINYA SUZU,[1] MASATERU HIYOSHI,[1] NAOKO TAKAHASHI-MAKISE,[1] TAKAMASA UENO,[2] TSUTOMU AGATSUMA,[3] HIROFUMI AKARI,[4] JUN KOMANO,[5] YUTAKA TAKEBE,[6] KAZUO MOTOYOSHI,[7] AND SEIJI OKADA[1]*

[1]*Division of Hematopoiesis, Center for AIDS Research, Kumamoto University, Kumamoto, Kumamoto, Japan*

[2]*Viral Immunology, Center for AIDS Research, Kumamoto University, Kumamoto, Kumamoto, Japan*

[3]*Tokyo Research Laboratories, Kyowa Hakko Co., Ltd, Machida, Tokyo, Japan*

[4]*Laboratory of Disease Control, Tsukuba Primate Research Center, National Institute of Biomedical Innovation, Tsukuba, Ibaraki, Japan*

[5]*Laboratory of Virology and Pathogenesis, AIDS Research Center, National Institute of Infectious Diseases, Shinjuku, Tokyo, Japan*

[6]*Laboratory of Molecular Biology and Epidemiology, AIDS Research Center, National Institute of Infectious Diseases, Shinjuku, Tokyo, Japan*

[7]*Department of Internal Medicine, National Defense Medical College, Tokorozawa, Saitama, Japan*

HIV-1 Nef accelerates the progression to AIDS by binding with and activating a Src kinase Hck, but underlying molecular basis is not understood. We revealed that Nef disturbed *N*-glycosylation/trafficking of a cytokine receptor Fms in an Hck-dependent manner, a possible trigger to worsen uncontrolled immune system. Here, we provide direct evidence that dys-regulated activation of Hck pre-localized to the Golgi apparatus causes this Fms maturation arrest. A striking change in Hck induced by Nef other than activation was its skewed localization to the Golgi due to predominant Golgi-localization of Nef. Studies with different Nef alleles and their mutants showed a clear correlation among higher Nef-Hck affinity, stronger Hck activation, severe Golgi-localization of Hck and severe Fms maturation arrest. Studies with a newly discovered Nef-Hck binding blocker 2c more clearly showed that skewed Golgi-localization of active Hck was indeed the cause of Fms maturation arrest. 2c blocked Nef-induced skewed Golgi-localization of an active form of Hck (Hck-P2A) and Fms maturation arrest by Nef/Hck-P2A, but showed no inhibition on Hck-P2A kinase activity. Our finding establishes an intriguing link between the pathogenesis of Nef and a newly emerging concept that the Golgi-localized Src kinases regulate the Golgi function.

J. Cell. Physiol. 221: 458–468, 2009.

Studies of HIV-1-infected patients and monkey models have demonstrated that Nef, a protein with no enzymatic activity encoded by the HIV-1 genome, is a critical determinant for the development of AIDS (Kestler et al., 1991; Deacon et al., 1995; Kirchhoff et al., 1995). Subsequent studies of HIV-1 transgenic (Tg) mice supported the idea. The expression of entire coding sequences of HIV-1 in $CD4^+$ T cells and macrophages caused an AIDS-like disease, which was abolished by Nef deletion (Hanna et al., 1998). This pathogenetic activity of Nef is supposed to be mediated by its binding with cellular proteins, and a well-defined partner of Nef is Hck (Saksela et al., 1995), a member of Src family tyrosine kinases expressed in macrophages. Other Src kinases (Lyn, Fyn, c-Src, and Lck) bind Nef but with lower affinities (Arold et al., 1998; Karkkainen et al., 2006; Trible et al., 2006). Importantly, the disruption of proline-rich PxxP motif of Nef, an essential motif to bind the Src homology 3 (SH3) domain of Hck, was sufficient to protect Tg mice from the AIDS-like disease, and wild-type Nef-induced disease progression was significantly delayed in $Hck^{-/-}$ mice (Hanna et al., 2001), indicating that high affinity Nef-Hck binding in macrophages is at least in part responsible for disease development and progression. However, unresolved issue is how Nef-Hck binding followed by activation of Hck (Moarefi et al., 1997; Lerner and Smithgall, 2002) satisfactorily account for disease development and progression.

An important clue to the issue is that Nef predominantly localized to the Golgi apparatus (Greenberg et al., 1998; Drakesmith et al., 2005; Haller et al., 2007) and that Nef not only activated Hck but also induced skewed localization of Hck to the Golgi (Hung et al., 2007). The Golgi functions as a sorting hub and location of glycosylation for proteins, and several lines of evidence have revealed that Src kinases, shown to be involved in a wide array of intracellular signaling (reviewed in

Contract grant sponsor: Ministry of Education, Culture, Sports, Science and Technology of Japan.
Contract grant sponsor: Human Science Foundation, Japan.

*Correspondence to: Seiji Okada, Division of Hematopoiesis, Center for AIDS Research, Kumamoto University, Kumamoto 860-0811, Japan. E-mail: okadas@kumamoto-u.ac.jp

Received 17 February 2009; Accepted 11 June 2009

Published online in Wiley InterScience (www.interscience.wiley.com.), 7 July 2009.
DOI: 10.1002/jcp.21878

Lowell, 2004), also play a role in the regulation of the Golgi structure/function. First, a fraction of Src kinases, including Hck, is physiologically found at the Golgi (David-Pfeuty and Nouvian-Dooghe, 1990; Kaplan et al., 1992; Ley et al., 1994; Bijlmakers et al., 1997; van't Hof and Resh, 1997; Carreno et al., 2000; Kasahara et al., 2004). Second, fibroblasts lacking three ubiquitous Src kinases (c-Src/Yes/Fyn) exhibited an aberrant Golgi structure composed of collapsed stacks and bloated cisternae (Bard et al., 2003). Third, an increased protein load entering the *cis*-Golgi from the endoplasmic reticulum activated the Golgi-localized Src kinases, which in turn regulated overall protein trafficking activity in the secretory pathway (Pulvirenti et al., 2008). Importantly, the study by Pulvirenti et al. indicates that coordinated regulation of activity of the Golgi-localized Src kinases is crucial to maintain the Golgi function, which raises an intriguing possibility that Nef affects protein trafficking process and thereby macrophage phenotype/function through skewed Golgi-localization of active Hck.

Indeed, we recently identified an aberrant function of Nef, which was possibly due to the skewed Golgi-localization of active Hck. We previously found that Nef inhibited the signal of M-CSF, a primary cytokine for macrophages (Suzu et al., 2005), which was a possible trigger to worsen uncontrolled immune systems in patients, as M-CSF is essential to maintain macrophages at an anti-inflammatory state (reviewed in Hamilton, 2008). Of interest was the role of Hck in this inhibitory activity of Nef (Hiyoshi et al., 2008). Nef reduced cell surface expression of M-CSF receptor Fms in myeloid cells and macrophages, which was the direct cause of the inhibitory activity of Nef on M-CSF signal. Importantly, such reduced cell surface expression of Fms was reproduced in transfected 293 cells, but only in co-expression with Hck. More importantly, the reduced cell surface expression was due to the accumulation of an immature under-*N*-glycosylated Fms at the Golgi (hereinafter called Fms maturation arrest). However, constitutive-active Hck alone failed to induce such Fms maturation arrest. These results indicate that Nef inhibits M-CSF signal by arresting Fms *N*-glycosylation and trafficking at the Golgi and that such Fms maturation arrest was not caused just because of Hck activation. Thus, a most likely cause of Nef-induced Fms maturation arrest was skewed Golgi-localization of active Hck. However, this intriguing hypothesis should be carefully and directly tested, because it will not only help to clarify molecular basis of this novel function of Nef through Hck, but also provide an excellent example of disease-associated failure of the Golgi function regulation by the Golgi-localized Src kinases.

In this study, we therefore sought to definitely conclude that skewed Golgi-localization of active Hck was indeed the direct cause of Fms maturation arrest by Nef. To this end, we employed two different approaches. First, we prepared various Nef proteins and compared their abilities to induce skewed Golgi-localization of Hck, Hck activation and Fms maturation arrest. Second and importantly, we discovered a small-molecule non-kinase inhibitor that effectively blocked Nef-Hck binding and performed mechanistic analyses with the newly discovered compound.

Materials and Methods

Expression plasmids

For the expression in HEK293 cells (Invitrogen, Carlsbad, CA), human Fms- and human p56Hck cDNA cloned into pCDNA3.1 vector (Invitrogen) were used (Suzu et al., 2005; Hiyoshi et al., 2008). The constitutive-active Hck P2A mutant (Hiyoshi et al., 2008) was also used in selected experiments. The expression plasmid for human Lyn cloned in pME-puro vector was provided by Y. Yamanashi (Tokyo Medical and Dental University, Tokyo, Japan) and used in the pull-down assay with GST-Nef fusion proteins (see below). Nef cDNA derived from the NL43 or SF2 strain of HIV-1 was cloned into pRc/CMV-CD8 vector to express the extracellular/transmembrane regions of CD8-Nef fusion protein (Hiyoshi et al., 2008). NL43 Nef-M20A was prepared as described previously (Akari et al., 2000). NL43 Nef-AxxA and $-\Delta E$ mutant were provided by A. Adachi (University of Tokushima, Tokushima, Japan) and J.C. Guatelli (University of California, San Diego, CA), respectively. In this study, we prepared another NL43 Nef mutant (NL43 Nef-TR), by using QuikChange II Site-directed Mutagenesis Kits (Stratagene, La Jolla, CA). We also prepared Nef constructs expressing Nef-GFP fusion proteins (Ueno et al., 2008). For the expression of GST-Nef fusion proteins, fragments containing the entire coding sequences of the wild-type NL43 Nef, NL43 Nef-TR mutant, wild-type SF2 Nef, and SF2 Nef-AxxA mutant were subcloned into pGEX-6P-1 vector (GE Healthcare, Buckinghamshire, UK). SF2 Nef-AxxA mutant was prepared by using QuikChange II Site-directed Mutagenesis Kits (Stratagene). The nucleotide sequences of the coding region of all Nef constructs were verified by using BigDye Terminator v3.1 Cycle Sequencing Kit (Applied Biosystems, Foster City, CA) and ABI PRISM 3100 Genetic Analyzer (Applied Biosystems).

Chemicals

PP2 (Sigma, San Diego, CA) was used as the Src kinase inhibitor. UCS15A and its synthetic derivatives, 2b and 2c, were prepared as described (Oneyama et al., 2003). All these inhibitors were dissolved in dimethyl sulfoxide (DMSO; Wako, Osaka, Japan).

Western blotting

HEK293 cells were maintained with DME medium (Wako) supplemented with 10% fetal calf serum (FCS). The maturation of Fms proteins or the activation of Hck was analyzed by the transient expression assay with the cells followed by Western blotting as described previously (Suzu et al., 2005; Hiyoshi et al., 2008). In brief, cells grown on a 12-well tissue culture plate were transfected with plasmid for Fms (0.4 μg), Nef (0.8 μg), or Hck (0.4 μg) in the combinations indicated using LipofectAMINE2000 reagent (Invitrogen), unless otherwise stated. Total amounts of plasmids were normalized with the empty vectors. After 6 h, culture medium was replaced with complete medium and the transfected cells were cultured for an additional 42 h. In selected experiments, chemicals such as PP2 and 2c were added to the culture at the same time of changing medium. Total cell lysates were prepared essentially as described (Suzu et al., 2000). Primary antibodies used for Western blotting were as follows: anti-Fms (C-20; Santa Cruz Biotechnology, Santa Cruz, CA), anti-CD8 (H-160; Santa Cruz), anti-GFP (FL; Santa Cruz), anti-Hck (clone 18; Transduction Laboratories, Lexington, KY), anti-Hck phosphorylated at tyrosine 411 (Hck-pTyr^{411}; Santa Cruz), anti-phosphotyrosine (PY99; Santa Cruz), and anti-ERK1/2 (K-23; Santa Cruz). The relative intensity of bands on scanned gel images was quantified using NIH Image software, and the Fms maturation arrest or Hck activation is also shown graphically on an arbitrary unit. The relative intensity of bands on Hck-pTyr^{411} blots was quantified and the degree of Hck activation was expressed as a fold-increase relative to the control. For Fms maturation arrest, we calculated the percentage of immature under-*N*-glycosylated Fms of total Fms protein amount, and compared the percentages among samples.

Immunofluorescence

The signal of Nef-GFP was directly visualized with a BZ-8000 fluorescent microscope (Keyence, Osaka, Japan) equipped with Plan-Fluor ELWD 20x/0.45 objective lenses (Nikon, Tokyo, Japan) (Hiyoshi et al., 2008). To detect active Hck, cells were fixed in 2% paraformaldehyde, permeabilized with ethanol, and stained with goat anti-active Hck antibodies (Santa Cruz). Secondary antibodies were anti-goat IgG-AlexaFluo488 (Molecular Probes, Eugene, OR). Nuclei were stained with DAPI (Molecular Probes), and

fluorescent signals were visualized as above. Image processing was performed using BZ-analyzer (Keyence) and Adobe Photoshop Software (Adobe Systems, San Jose, CA).

GST pull-down

The control GST or GST-Nef fusion proteins (wild-type NL43 Nef, NL43 Nef-TR, wild-type SF2 Nef, and SF2 Nef-AxxA) cloned in pGEX-6P-1 vector was expressed in *E. coli* BL21 cells (GE Healthcare). Cells were grown in LB media containing 50 μg/ml ampicillin followed by induction with 1 μM IPTG. The expression-induced cells were harvested and lysed with BugBuster Protein Extraction Reagent containing 1 U/ml rLysozyme and 25 U/ml Benzonaze Nuclease (Novagen, Madison, WI). The cleared lysates were then incubated with GST-Bind Resin (Novagen). After extensive washing with GST Bind/Wash Buffer (Novagen), the resin was incubated with the total cell lysates of HEK293 cells transfected with the expression plasmid for Hck or Lyn. In a selected experiment, 2c was added to the mixtures. After extensive re-washing, the resin was boiled with SDS–PAGE sample buffer and elutes were analyzed for the presence of Hck or Lyn by western blotting. Primary antibodies used were as follows (both from Transduction Laboratories): anti-Hck (clone 18) and anti-Lyn (clone 42). In a selected experiment, we also used GST proteins fused to the SH3 domain of Hck (Paliwal et al., 2007), which was provided by G. Swarup (Center for Cellular and Molecular Biology, Hyderabad, India).

Subcellular fractionation

The subcellular fractionation on sucrose gradients was performed exactly as reported (Matsuda et al., 2006). In brief, cells were

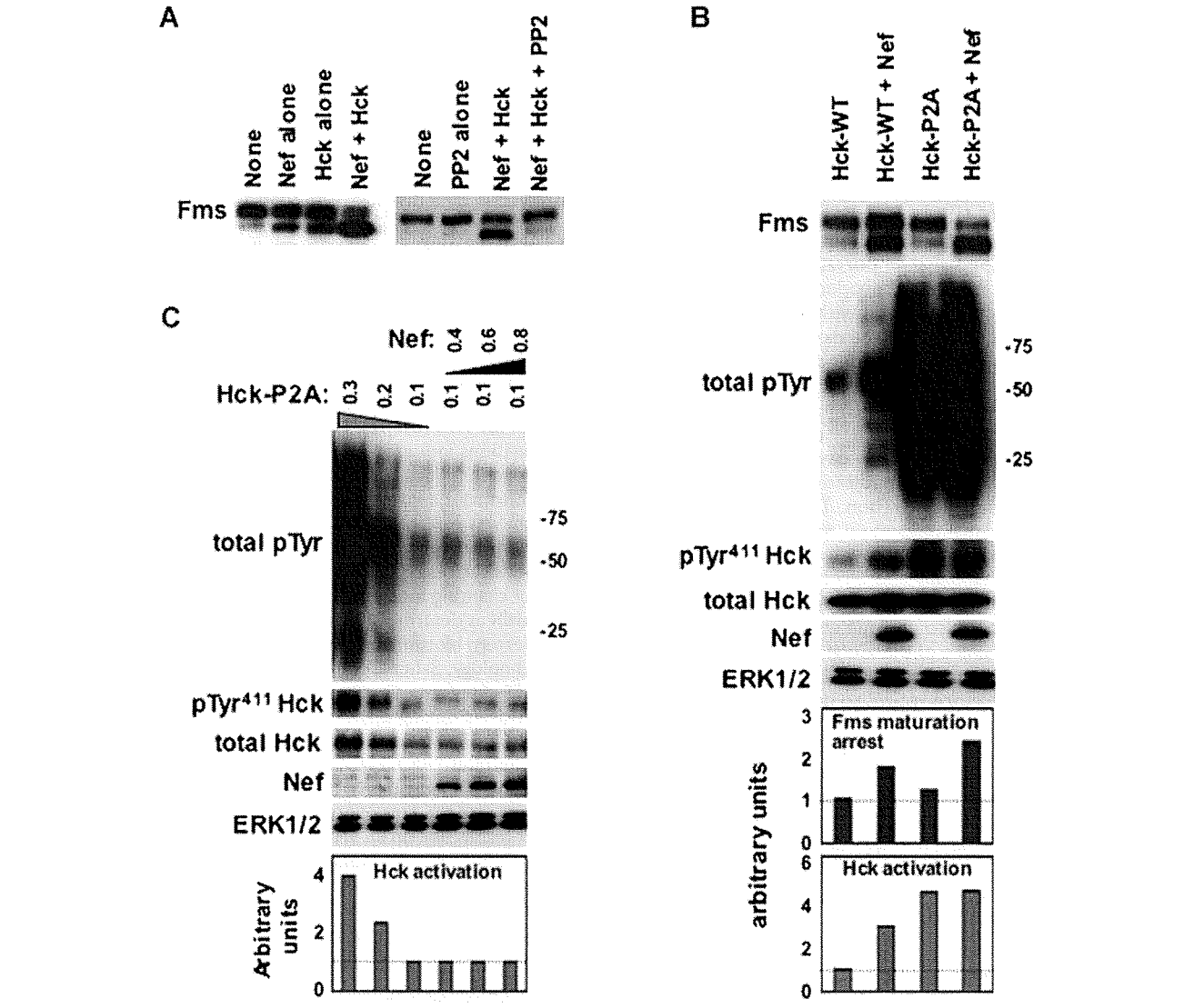

Fig. 1. Nef/Hck-induced Fms mturation arrest. A: HEK293 cells were transfected with Fms plamid alone (None) or co-transfected with the plasmids for NL43 Nef and/or wild-type Hck as indicated. In the right blot, PP2 was added to selected wells at a final concentration of 10 μM after the transfection, Total cell lysates were subjected to Fms Western blotting. B: Cells were transfected with Fms plasmid alone (None) or in combination with the plasmids for Nef (NL43) and Hck (WT or constitutive-active P2A), as indicated. These cells were then analyzed for the expression of Fms, tyrosine-phosphorylated proteins (total pTyr), active-Hck (pTyr^{411}Hck), total Hck, CD8-Nef (Nef), or ERK by Western blotting. The ERK blot is a loading control. The quantified Fms maturation arrest and Hck activation are shown in the bar graphs. C: Cells were transfected with varying amounts (μg) of Hck-P2A and NL43 Nef plasmids as indicated, and analyzed as in (B). The quantified Hck activation is shown in the bar graphs. [Color figure can be viewed in the online issue, which is available at www.interscience.wiley.com.]

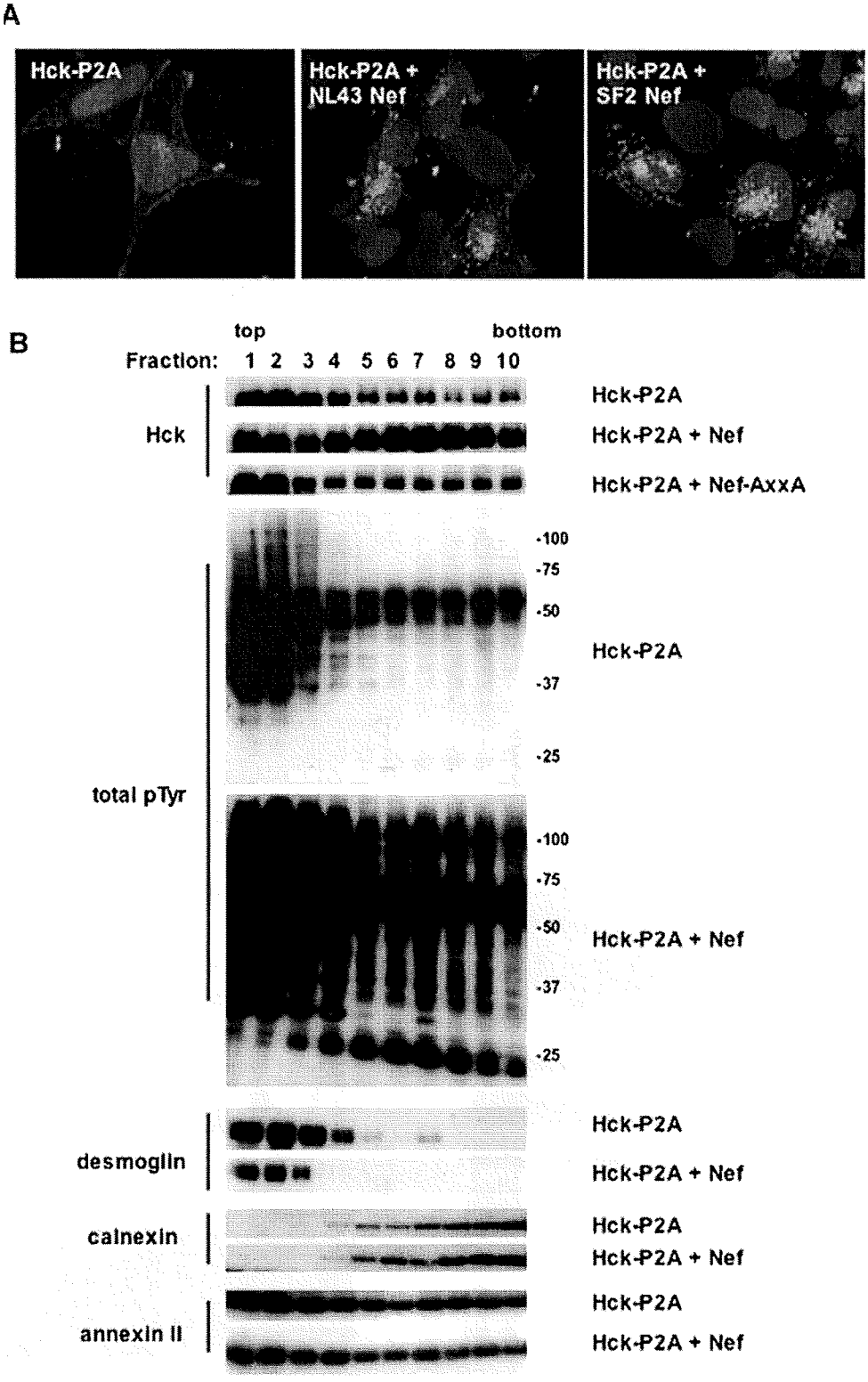

Fig. 2. Skewed Golgi-localization of Hck by Nef. A: HEK293 cells were transfected with Hck-P2A plasmid alone, or co-transfected with NL43 Nef or SF2 Nef plasmid. Cells were stained with antibody specific for active Hck (green) and DAPI (blue). B: Cells were transfected with Hck-P2A alone, or co-transfected with NL43 Nef. Then, cells were subjected to subcellular fractionation on sucrose gradients and Western blotting with antibodies against Hck, phosphotyrosine (pTyr), desmoglein, calnexin, or annexin II. [Color figure can be viewed in the online issue, which is available at www.interscience.wiley.com.]

swollen in hypotonic buffer containing protease inhibitors followed by homogenization. Then, the post-nuclear supernatants were fractionated by ultracentrifugation on discontinuous sucrose gradients. All steps were carried out on ice. The fractions obtained were subjected to Western blotting with antibodies to Hck (clone 18; Transduction Laboratories), desmoglein (clone 62; Transduction Laboratories), annexin II (C-10; Santa Cruz), or calnexin (H-70; Santa Cruz).

Flow cytometry

Human myeloid TF-1-fms cells expressing Nef-ER fusion protein were maintained as described previously (Suzu et al., 2005; Hiyoshi et al., 2008). To activate the Nef-ER fusion protein, we used the estrogen analog 4-HT (Sigma) at a final concentration of 0.1 μM. The cells were stained with PE-labeled anti-Fms antibodies (Santa Cruz), and the level of cell surface Fms was analyzed by flow cytometry on a FACS Calibur using Cell Quest software (Becton Dickinson, Mountain View, CA).

Results

Analyses with Src kinase inhibitor and Hck mutant

As reported, Nef induces Fms maturation arrest when co-expressed with Hck in HEK293 cells (Fig. 1A). HEK293 cells do not express Hck endogenously, and the upper and lower band was the fully *N*-glycosylated and under-*N*-glycosylated Fms, respectively (Hiyoshi et al., 2008). The low molecular weight Fms was sensitive to Endo-H (Endo-β-*N*-acetylglucosaminindase H), which selectively cleaves high-mannose type oligosaccharide, and their increase was clearly associated with the intense staining of Fms mainly at

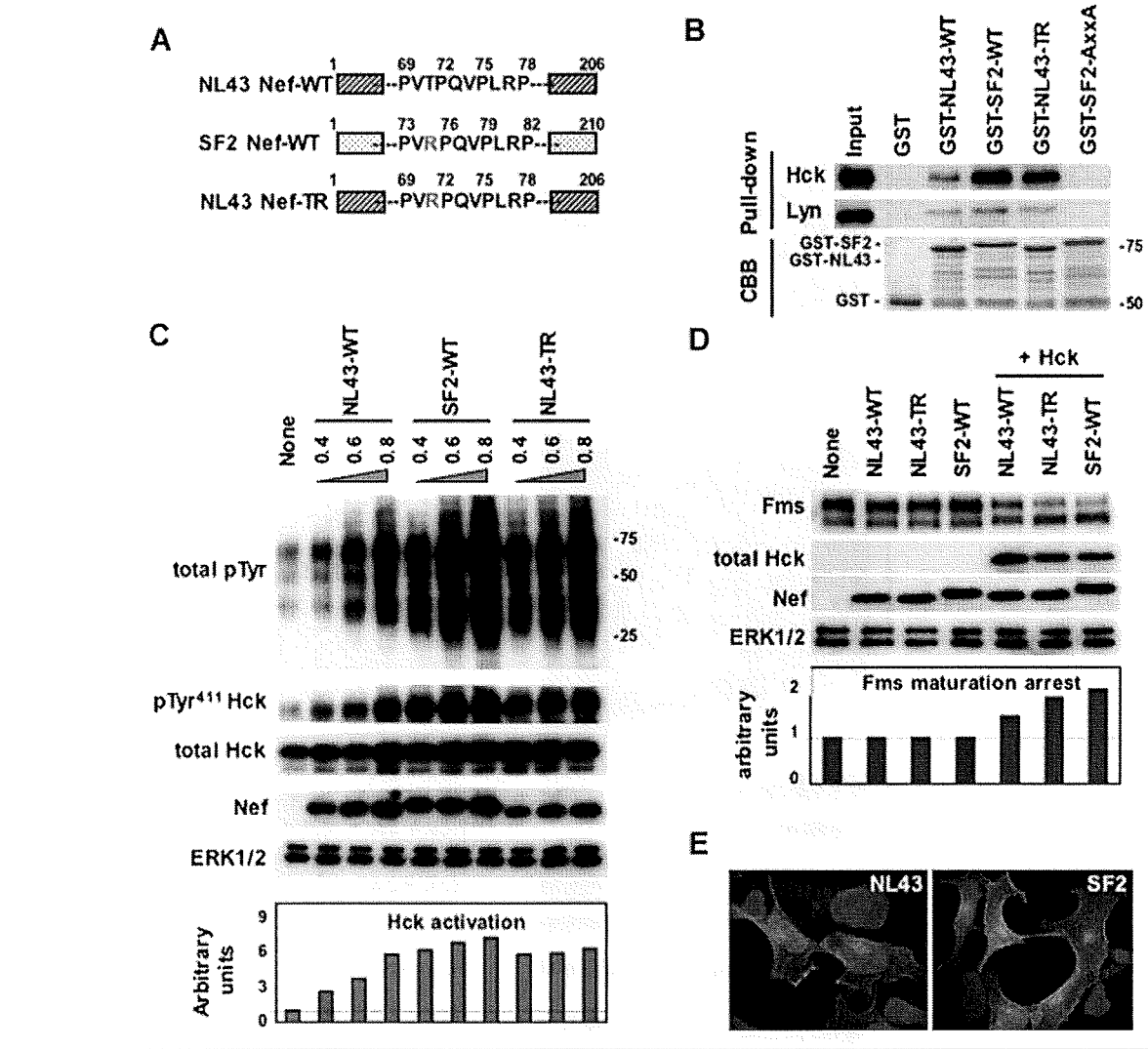

Fig. 3. Abilities of different Nef alleles to bind/activate Hck and to induce Fms maturation arrest. A: The NL43 Nef, SF2 Nef, and NL43 Nef-TR mutant used are schematically shown. B: The resins, to which the control GST or indicated GST-Nef proteins were bound, were incubated with the lysates of HEK293 cells expressing Hck or Lyn. The amount of Hck or Lyn bound to the resins was determined by Western blotting (Pull-down). The amount of GST and GST-Nef fusion proteins bound to the resins was verified by the elution from the resins followed by SDS–PAGE/Coomassie brilliant blue (CBB) staining. C: HEK293 cells were co-transfected with the wild-type Hck and indicated Nef alleles. The amounts of Nef plasmids used are shown (0.4, 0.6, or 0.8 μg/well). Total cell lysates were subjected to Western blotting with antibodies against phosphotyrosine (total pTyr), active-Hck (pTyr^{411}Hck), total Hck, CD8-Nef (Nef), or ERK by Western blotting. The quantified Hck activation is shown in the bar graph. D: Cells were transfected with Fms plasmid alone (None) or in combination with the plasmids for Nef and Hck, as indicated. Western blotting was done as in (C). E: Cells were transfected with indicated GFP-Nef plasmid (green). Nuclei were stained with DAPI (blue). [Color figure can be viewed in the online issue, which is available at www.interscience.wiley.com.]

the perinuclear region, which overlapped well with the signal of GM130 or Vti1a, the markers for the Golgi (Hiyoshi et al., 2008). These results strongly suggested that the low molecular weight Fms was the immature under-*N*-glycosylated form. The increase of the lower molecular weight species was obvious in the cells co-expressing Nef and Hck (Fig. 1A, left blot), and this Fms maturation arrest was blocked by a Src kinase inhibitor PP2 (Fig. 1A, right blot). However, the expression of a constitutive-active Hck mutant (Hck-P2A; Lerner and Smithgall, 2002) was not sufficient to induce Fms maturation arrest when expressed alone (Fig. 1B, Fms blot), despite its strong kinase activity (total pTyr and $pTyr^{411}$ Hck blots). In this study, we monitored kinase activity of Hck by overall protein tyrosine-phosphorylation (total pTyr) and auto-phosphorylation of Hck ($pTyr^{411}$ Hck) (reviewed in Korade-Mirnics and Corey, 2000). Nonetheless, Hck-P2A/Nef co-expression induced more severe Fms maturation arrest than wild-type Hck/Nef co-expression (Fig. 1B), and Nef did not enhance the kinase activity of Hck-P2A (Fig. 1C), confirming our previous finding that Hck activation was necessary but not sufficient for Nef-induced Fms maturation arrest.

Analyses with different Nef alleles and their mutants

In this study, we first found that Nef derived from SF2 strain of HIV-1 induced more severe Golgi-localization of Hck-P2A than Nef derived from NL43 strain. Hck-P2A signal at the plasma membrane was still observed in some NL43 Nef-transfected cells, whereas such signal was not observed in SF2 Nef-transfected cells (Fig. 2A). The Nef-induced skewed Golgi-localization of Hck-2PA was confirmed by a quantitative analysis, that is, subcellular fractionation on sucrose gradients. Based on a previous report (Matsuda et al., 2006), we used desmoglein, annexin II and calnexin as marker proteins for the plasma membrane, both the plasma membrane and the Golgi, and the endoplasmic reticulum, respectively. As shown (Fig. 2B), the plasma membrane was recovered in light fractions whereas the Golgi and the endoplasmic reticulum were recovered in heavy fractions, and the peak of Hck-P2A shifted to heavy fractions by the co-expression with NL43 Nef but not a Nef-AxxA mutant defective in the binding to Hck (Saksela et al., 1995). The peak shift was also associated with the appearance of many tyrosine-phosphorylated proteins in these fractions (Fig. 2B).

Both NL43 Nef and SF2 Nef had intact PxxP motif (Fig. 3A), but SF2 Nef showed much higher affinity to Hck than NL43 Nef (Fig. 3B). In the control experiments, we confirmed that the binding of both Nef to Lyn remained low and the PxxP motif-disrupted SF2 Nef mutant (AxxA) bound neither Hck nor Lyn. Reflecting the higher affinity to Hck, SF2 Nef induced stronger Hck activation (Fig. 3C) and more severe Fms maturation arrest (Fig. 3D). As expected, even SF2 Nef failed to induce Fms maturation arrest when co-expressed with Lyn (data not shown). However, SF2 Nef and NL43 Nef showed no obvious change in the pattern of predominant Golgi-localization (Fig. 3E). It was therefore likely that SF2 Nef bound Hck at

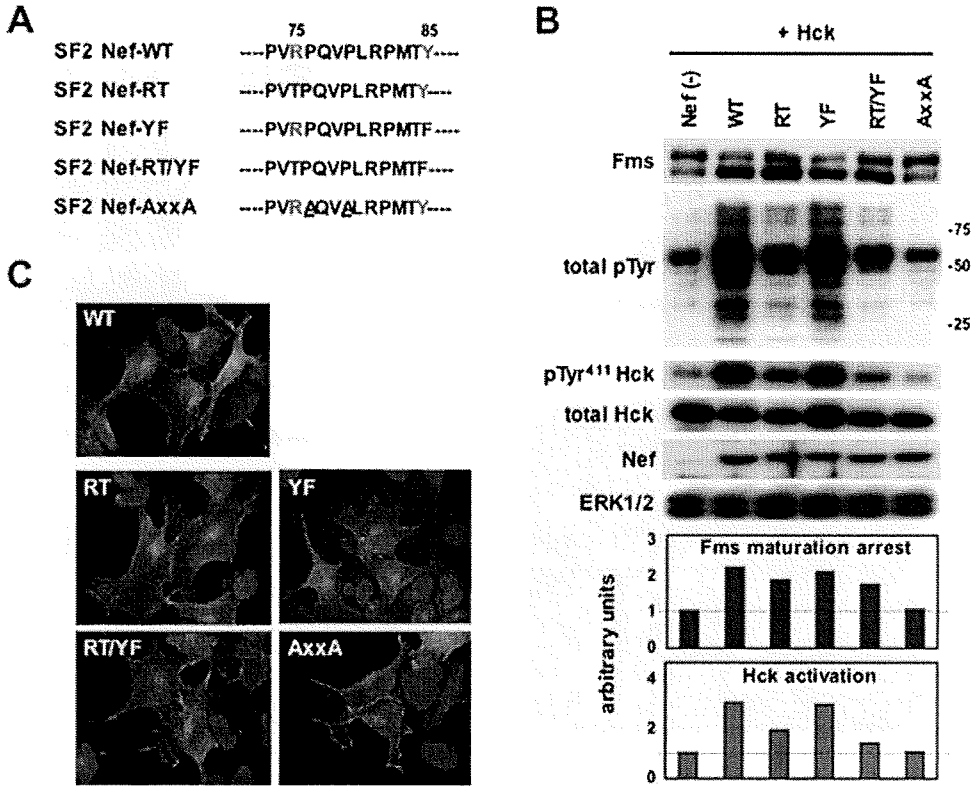

Fig. 4. Abilities of SF2 Nef mutants to activate Hck and to induce Fms maturation arrest. A: The SF2 Nef mutants used (RT, YF, RT/YF, and AxxA) are schematically shown. B: HEK293 cells were transfected with Fms plasmid alone (None) or in combination with the plasmids for Nef and Hck, as indicated. These cells were then analyzed for the expression of Fms, phosphotyrosine (total pTyr), active-Hck ($pTyr^{411}$Hck), total Hck, GFP-Nef (Nef), or ERK by Western blotting. The quantified Fms maturation arrest and Hck activation are shown in the bar graphs. C: Cells were transfected with indicated GFP-Nef plasmid (green). Nuclei were stained with DAPI (blue). [Color figure can be viewed in the online issue, which is available at www.interscience.wiley.com.]

the Golgi with higher affinity and thereby induced stronger Hck activation and more severe Fms maturation arrest.

There was a single amino acid difference within the PxxP motif, Thr^{71} in NL43 Nef and Arg^{75} in SF2 Nef (Fig. 3A). We found that an NL43 Nef with $Thr^{71}Arg$ substitution (NL43 Nef-TR) showed higher affinity to Hck than wild-type NL43 Nef (Fig. 3B), and induced stronger Hck activation (Fig. 3C) and more severe Fms maturation arrest (Fig. 3D) than wild-type NL43 Nef. We also performed a complementary experiment with SF2 Nef mutants (Fig. 4A; Ueno et al., 2008). As a result, we found that mutants with $Arg^{75}Thr$ substitution (SF2 Nef-RT and SF2-RT/YF) induced moderate Hck activation/Fms maturation arrest (Fig. 4B). However, both showed no obvious change in the pattern of predominant Golgi-localization (Fig. 4C). These results indicated that the single amino acid difference (Thr to Arg) within the PxxP motif governed the higher ability of SF2 Nef to induce Golgi-localization and activation of Hck, and Fms maturation arrest.

Although PxxP motif is essential for Nef to bind Hck, a recent study showed that an acidic region of Nef facilitated Nef-Hck binding at the Golgi (Hung et al., 2007). Although an NL43 Nef mutant lacking this region (ΔE; Fig. 5A) bound GST-Hck SH3 fusion proteins as with wild-type NL43 Nef (Fig. 5B), ΔE mutant was indeed less active than wild-type in transfected HEK293 cells, that is, in both Hck and activation Fms maturation arrest (Fig. 5C). Another mutant (M20; Fig. 5A), which was defective in the down-regulation of MHC I, another hallmark function of Nef (Akari et al., 2000), retained the ability to induce Hck activation and Fms maturation arrest (Fig. 5C). Both ΔE and M20A mutants showed no obvious change in the pattern of predominant Golgi-localization (Fig. 5C). The result further supported the idea that stronger Hck activation, which took place at the Golgi, induced severe Fms maturation arrest.

Analyses with a newly discovered Nef-Hck binding blocker

To directly show that the Golgi-localization of active Hck determines Nef-induced Fms maturation arrest, we sought to discover Nef-Hck binding blockers. In this study, we focused on UCS15A and its analogs 2b and 2c (Fig. 6A), because these small-molecule compounds were shown to block several proline-rich motif-SH3 domain binding such as Sam68-Fyn binding (Oneyama et al., 2003) and AMAP1-cortactin binding (Hashimoto et al., 2006). As they have not been used before for HIV-1 studies, we tested their capability to block Nef-Hck binding by the GST pull-down assay. As shown (Fig. 6B), all compounds blocked the binding of Hck to NL43 Nef or NL43 Nef-TR mutant (more potent than the wild-type, see Fig. 3), in a dose-dependent manner. Like the case of Sam68-Fyn binding (Oneyama et al., 2003), 2c was the most effective in blocking Nef-Hck binding (Fig. 6B), and showed no obvious toxicity to HEK293 cells (Fig. 6C). As shown (Fig. 6D), 2c indeed inhibited

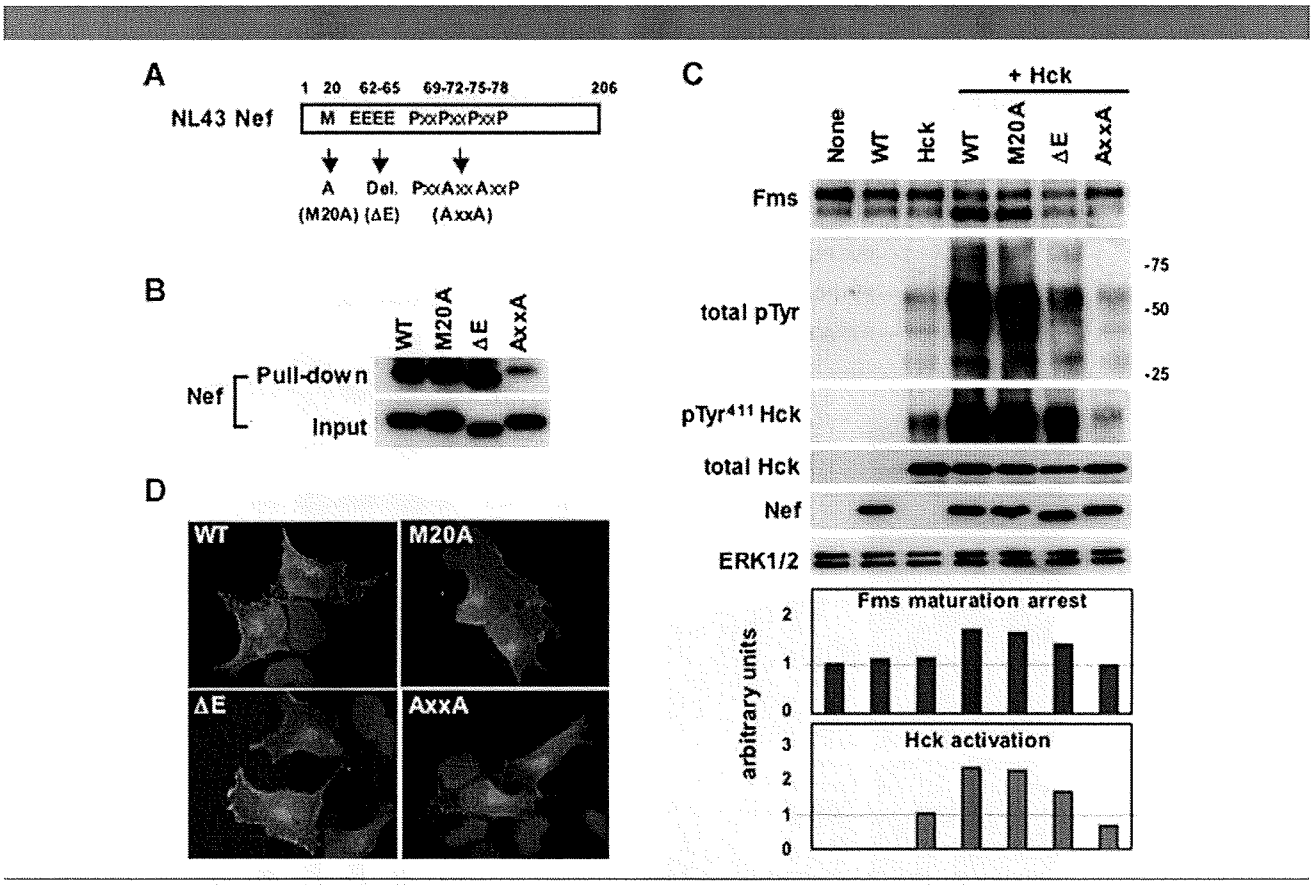

Fig. 5. Abilities of NL43 Nef mutants to activate Hck and to induce Fms maturation arrest. A: The NL43 Nef mutants used (M20A, ΔE, and AxxA) are schematically shown. B: The resin, to which GST-Hck SH3 fusion proteins were bound, were incubated with the lysates of HEK293 cells expressing the indicated Nef proteins. The amount of Nef proteins in the lysates (Input) or bound to the resins (Pull-down) was verified by Western blotting. C: HEK293 cells were transfected with Fms plasmid alone (None) or in combination with the plasmids for Nef and Hck, as indicated. These cells were then analyzed for the expression of Fms, phosphotyrosine (total pTyr), active-Hck ($pTyr^{411}$ Hck), total Hck, CD8-Nef (Nef), or ERK by Western blotting. The quantified Fms maturation arrest and Hck activation are shown in the bar graphs. D: Cells were transfected with indicated GFP-Nef (green). Nuclei were stained with DAPI (blue). [Color figure can be viewed in the online issue, which is available at www.interscience.wiley.com.]

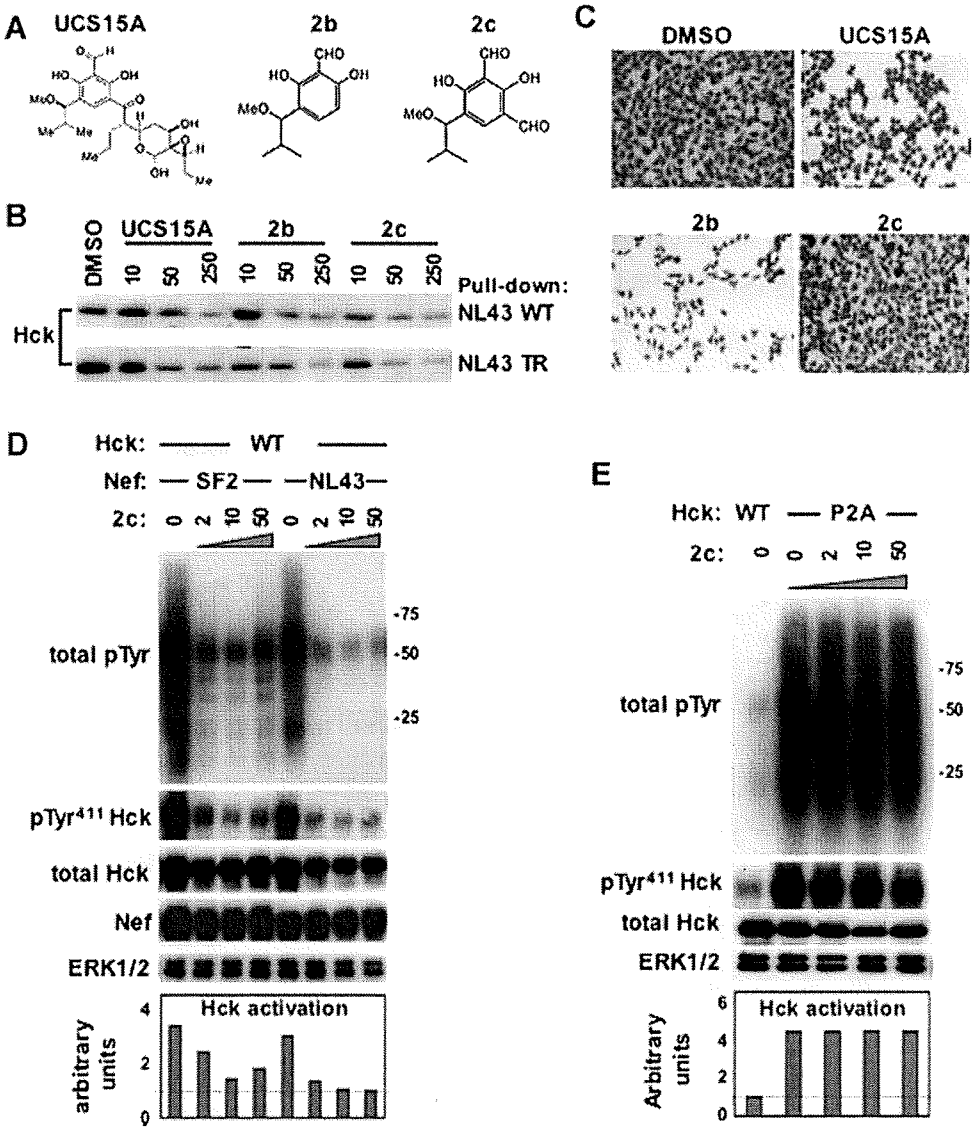

Fig. 6. Capability of 2c to block Nef-Hck binding and Nef-induced Hck activation. A: Chemical structures of UCS15A, 2b, and 2c are shown. B: The resins, to which GST-Nef (NL43 wild-type or TR mutant, see Fig. 2A) proteins were bound, were incubated with the lysates of Hck-expressing HEK293 cells in the absence (DMSO) or presence of the indicated concentration (0, 10, 50, or 250 μM) of UCS15A, 2b, or 2c. The amount of Hck proteins bound to the resins was determined by Western blotting. C: HEK293 cells were cultured in the absence (DMSO) or presence of 50 μM of UCS15A, 2b, or 2c for 2 days, and subjected to Wright-Giemsa staining. D: Cells were co-transfected with Hck-WT and indicated Nef alleles (SF2 or NL43), and cultured in the presence of increasing concentrations (μM) of 2c. These cells were then analyzed for the expression of tyrosine-phosphorylated proteins (total pTyr), active-Hck (pTyr^{411}Hck), total Hck, CD8-Nef (Nef), or ERK by Western blotting. The quantified Hck activation is shown in the bar graphs. E: Cells were transfected with Hck-WT or Hck-P2A, and cultured in the presence of increasing concentrations (μM) of 2c. These cells were analyzed as in (D). [Color figure can be viewed in the online issue, which is available at www.interscience.wiley.com.]

Hck activation by NL43 Nef and more potent SF2 Nef (see Fig. 3). Importantly, 2c had little inhibitory effect on kinase activity of the constitutive-active Hck P2A mutant, even when used at a concentration as high as 50 μM (Fig. 6E). These results indicated that 2c was not a kinase inhibitor but inhibited Nef-induced Hck activation by blocking Nef-Hck binding.

This unique feature of 2c prompted us to examine whether 2c blocks Nef/Hck-induced Fms maturation arrest and Nef-induced skewed Golgi-localization of Hck. As shown (Fig. 7A), 2c completely blocked Fms maturation arrest induced by Nef and wild-type Hck as expected. However, of particular importance was that 2c also completely blocked severe Fms maturation arrest induced by Nef and the constitutive-active Hck P2A (Fig. 7B). Because 2c had little inhibitory effect on kinase activity of Hck-P2A (see Fig. 6E), these results strongly supported that the presence of Hck-P2A at the Golgi caused by its binding with Nef (see Fig. 2) was a direct cause of severe Fms maturation arrest. We therefore sought to verify that 2c indeed blocked Nef-induced skewed Golgi-localization of Hck-P2A. To this end, we employed the quantitative analysis, that is, subcellular fractionation on sucrose gradients (see Fig. 2B). The peak of Hck-P2A shifted to heavier fractions by the co-expression with Nef, and such change in the intracellular localization of Hck-P2A was restored to normal by the addition of 2c (Fig. 7C). We also tested whether 2c blocked Nef-induced Fms abnormality in another culture system. We previously showed that the cell surface expression of Fms was impaired in human myeloid TF-1-fms cells expressing a conditionally active

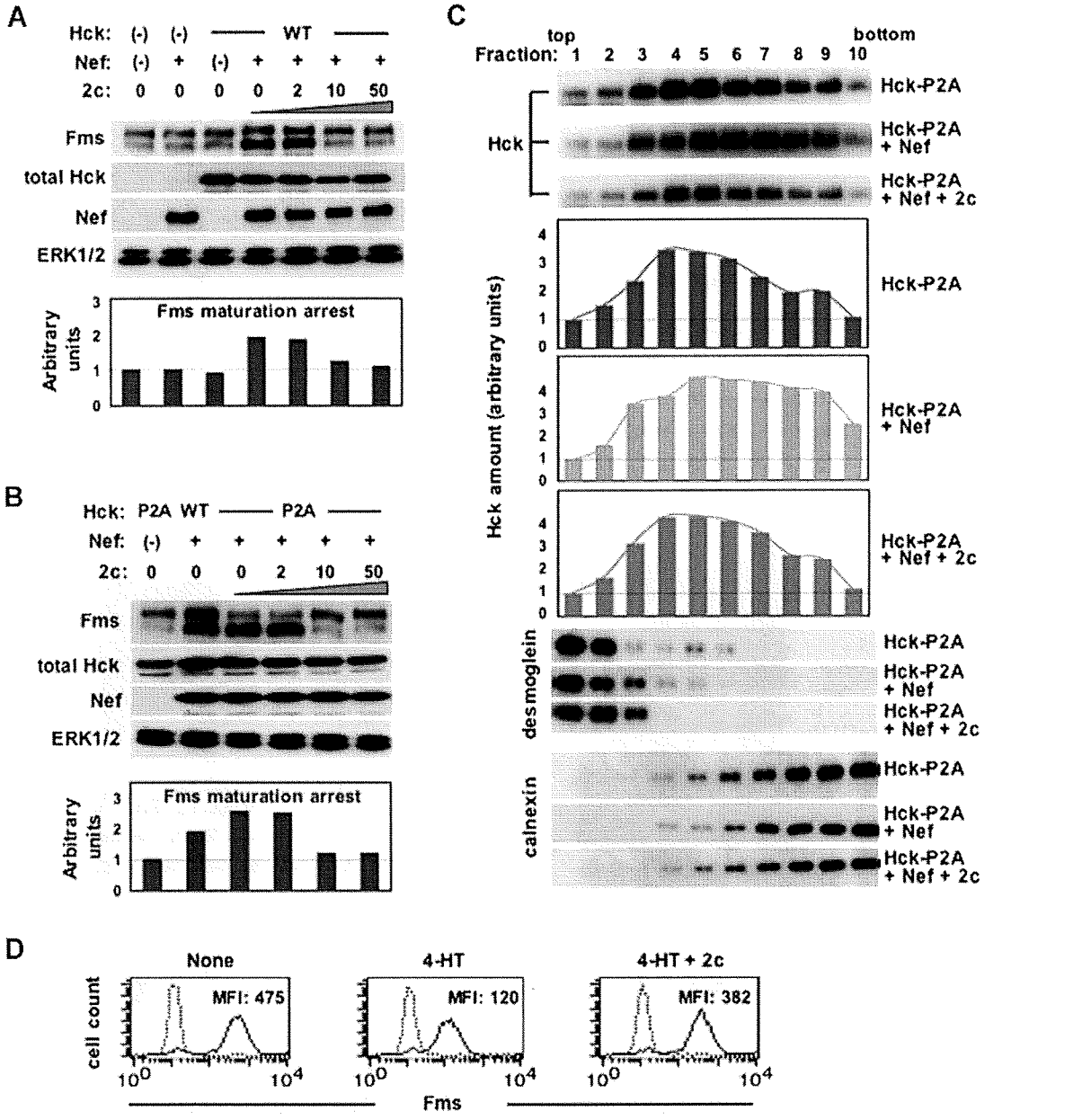

Fig. 7. Capability of 2c to block Fms maturation arrest and skewed Golgi-localization of Hck. A: HEK293 cells were transfected with the plasmids (Fms, NL43 Nef, and Hck-WT) in combination indicated, and cultured in the presence of increasing concentrations (μM) of 2c. These cells were then analyzed for the expression of Fms, total Hck, CD8-Nef (Nef), or ERK by Western blotting. The quantified Fms maturation arrest is shown in the bar graphs. B: Cells were transfected with the plasmids (Fms, NL43 Nef, Hck-WT, and Hck-P2A) in combination indicated, and cultured in the presence of increasing concentrations (μM) of 2c. These cells were then analyzed as in A. C: Cells were transfected with Hck-P2A alone (top), or co-transfected with NL43 Nef (middle). 2c was added to a final concentration of 50 μM to selected wells (bottom). Then, cells were subjected to subcellular fractionation on sucrose gradients and Hck Western blotting. The quantified Hck amounts are shown in the bar graph. The fractions were also analyzed for the amount of desmoglein and calnexin. D: TF-1-fms-Nef-ER cells cultured with M-CSF-free media in the absence (left) or presence of 0.1 μM 4-HT (middle), or the co-presence of 0.1 μM 4-HT and 50 μM 2c (right) for 12 h. The expression of Fms on the surface of treated cells was analyzed by flow cytometry with PE-labeled anti-Fms. The mean fluorescence intensity (MFI) of Fms expression is indicated. [Color figure can be viewed in the online issue, which is available at www.interscience.wiley.com.]

Nef-ER fusion protein when the Nef-ER in the cells was activated by the estrogen analog 4-HT (Hiyoshi et al., 2008). This impaired cell surface Fms expression was highly likely due to intracellular Fms maturation arrest (Hiyoshi et al., 2008). Finally, we found that the Fms down-regulation in Nef-active TF-1-fms-Nef-ER cells was also restored to normal by the addition of 2c (Fig. 7D). All taken together, our present study clearly demonstrated that skewed Golgi-localization of active Hck induced by Nef was indeed the direct cause of Fms maturation arrest.

Discussion

M-CSF is a cytokine essential not only for the survival of macrophages but also for the maintenance of macrophages at an

anti-inflammatory state (reviewed in Chitu and Stanley, 2006; Hamilton, 2008). Thus, the inhibitory effect of Nef on M-CSF signal through Fms maturation arrest at the Golgi is a possible trigger to worsen uncontrolled immune systems in patients (Suzu et al., 2005; Hiyoshi et al., 2008). In this study, we therefore sought to define molecular basis of this important function of Nef, by using different Nef alleles, various Nef mutants, constitutive-active Hck mutant, and Nef-Hck binding blocker 2c. The study with various Nef proteins supported the idea that high affinity Nef-Hck binding and subsequent stronger Hck activation, both of which took place mainly at the Golgi, determined Fms maturation arrest at the Golgi (Figs. 2–5). Moreover, the study with 2c enabled us to conclude that skewed Golgi-localization of active Hck by Nef was indeed the direct cause of Fms maturation arrest (Figs. 6 and 7). By analogy with the Sam68-Fyn binding inhibition (Oneyama et al., 2003), the inhibitory effect of 2c on Nef-Hck binding was supposed to be mediated by its interaction with Nef PxxP motif.

As mentioned earlier, it has been known for a long time that most members of Src kinases including Hck localize to the Golgi as well as to the plasma membrane. For example, it was shown that newly synthesized Lyn initially localized and accumulated to the Golgi, and then moved toward the plasma membrane (Kasahara et al., 2004). Importantly, Pulvirenti et al. (2008) recently revealed that coordinated regulation of activity of the Golgi-localized Src kinases is crucial to maintain intra-Golgi trafficking of proteins. Our present finding that skewed Golgi-localization of active Hck leads to Fms maturation arrest at the Golgi is in line with the new concept. It appears that long-lasting and dys-regulated activation of the Golgi-localized Src kinases disturbs glycosylation and/or trafficking of proteins, exemplified by Fms maturation arrest. Indeed, N-Src, a c-Src isoform with a higher basal tyrosine kinase activity (Brugge et al., 1985), showed more obvious perinuclear localization than the constitutive-active Hck-P2A and induced Fms maturation arrest even in the absence of Nef (unpublished result). Moreover, Mitina et al. (2007) reported that over-expression of an active form of Hck disturbed *N*-glycosylation of another cytokine receptor Flt3 even in the absence of Nef. These results may further support the idea that long-lasting and dys-regulated activation of the Golgi-localized Src kinases per se affects protein glycosylation and/or trafficking at the Golgi. Anyhow, our system with Nef provides a useful model to elucidate how Src kinases regulate the Golgi structure/function. It will be important to identify which Golgi proteins are phosphorylated directly or indirectly by Hck activated at the Golgi and to clarify how such phosphorylation cascade leads to Nef-induced Fms maturation arrest.

Nef has been shown to affect protein trafficking and a well-characterized target is major histocompatibility complex class I (MHC I). Nef reduced the cell surface expression of MHC I, which diminishes the recognition of infected cells by cytotoxic T cells (reviewed in Fackler and Baur, 2002; Peterlin and Trono, 2003). However, it is still in intense debate whether Nef requires SH3 domain-containing proteins such as Hck to reduce the cell surface level of MHC I (Schwartz et al., 1996; Greenberg et al., 1998; Mangasarian et al., 1999; Akari et al., 2000; Chang et al., 2001; Roeth and Collins, 2006; Hung et al., 2007; Atkins et al., 2008). In this regard, Fms is not the direct target of Nef. However, as shown, Nef disturbed the cell surface expression of Fms, which is triggered by skewed Golgi-localization of active Hck. Moreover, it was shown that Nef disturbed the cell surface expression of another macrophage-specific protein HFE, an iron homeostasis regulator, which was blocked by a dominant-negative Hck (Drakesmith et al., 2005). Although whether the reduced cell surface level of HFE by Nef relates to skewed Golgi-localization of active Hck is unclear, it is conceivable that Nef acquires an additional machinery to manipulate protein trafficking in macrophages by exploiting the Golgi-localized Hck. Of interest, the *N*-glycosylation of Flt3, which is structurally related to Fms, was also impaired in Nef/Hck-expressing HEK293 cells, but the degree of maturation arrest of Flt3 was quite weak when compared to that of Fms (data not shown). The finding may imply that Fms maturation arrest is not necessarily due to the general disruption in the Golgi structure or function. Future studies, in which we determine to what extent overall protein *N*-glycosylation and trafficking are affected by Nef-Hck binding, will further clarify pathological significance of the molecular binding in macrophages. The newly discovered Nef-Hck binding blocker 2c will be useful in such studies and may provide a strategy to complement current anti-HIV-1 therapy for better treatment outcomes.

In this study, we showed that SF2 Nef had much higher affinity to Hck than NL43 Nef and thereby induced stronger Hck activation/severe Golgi-localization of Hck (Figs. 2 and 3) and that the single amino acid difference (Thr^{71} in NL43 Nef and Arg^{75} in SF2 Nef) within PxxP motif largely governs the higher ability of SF2 Nef (Figs. 3 and 4). This difference might reflect that the $Thr^{71}Arg$ substitution in NL43 Nef (NL43 Nef-TR, see Fig. 3) altered the flexibility of a loop containing the PxxP motif (Fackler et al., 2001). Importantly, for reasons not clearly understood, NL43 Nef-TR was more pathogenic in HIV-1 Tg mice than wild-type NL43 Nef and the pathogenicity of SF2 Nef in Tg mice was evident despite very low levels of expression (Priceputu et al., 2007). It is therefore possible that more severe Golgi-localization of active Hck followed by perturbed *N*-glycosylation and trafficking of proteins including Fms account for the high pathogenicity of SF2 Nef in Tg mice.

In summary, our present study clearly demonstrated that skewed Golgi-localization of active Hck was the direct cause of Fms maturation arrest by Nef. Our findings establishes an intriguing link between the pathogenesis of HIV-1 Nef and the newly emerging concept that the Golgi-localized Src kinases regulate the Golgi function. The identification of Golgi proteins phosphorylated by the Golgi-localized active Hck will provide novel insights into molecular mechanisms by which Nef functions as an HIV-1 pathogenetic factor through Hck and the Gogi-localized Src kinases regulate the Golgi function.

Acknowledgments

We thank Dr. G. Thomas (Vollum Institute) for critical reading of the manuscript. We thank Ms. Y. Endo and Ms. I. Suzu for experimental assistance.

Literature Cited

Akari H, Arold S, Fukumori T, Okazaki T, Strebel K, Adachi A. 2000. Nef-induced major histocompatibility complex class I down-regulation is functionally dissociated from its virion incorporation, enhancement of viral infectivity, and CD4 down-regulation. J Virol 74:2907–2912.

Arold S, O'Brien R, Franken P, Strub MP, Hoh F, Dumas C, Ladbury JE. 1998. RT loop flexibility enhances the specificity of Src family SH3 domains for HIV-1 Nef. Biochemistry 37:14683–14691.

Atkins KM, Thomas L, Youker RT, Harriff MJ, Pissani F, You H, Thomas G. 2008. HIV-1 Nef binds PACS-2 to assemble a multikinase cascade that triggers major histocompatibility complex class I (MHC-I) down-regulation: Analysis using short interfering RNA and knock-out mice. J Biol Chem 283:11772–11784.

Bard F, Mazelin L, Pechoux-Longin C, Malhotra V, Jurdic P. 2003. Src regulates Golgi structure and KDEL receptor-dependent retrograde transport to the endoplasmic reticulum. J Biol Chem 278:46601–46606.

Bijlmakers MJ, Isobe-Nakamura M, Ruddock LJ, Marsh M. 1997. Intrinsic signals in the unique domain target p56lck to the plasma membrane independently of CD4. J Cell Biol 137:1029–1040.

Brugge JS, Cotton PC, Queral AE, Barrett JN, Nonner D, Keane RW. 1985. Neurones express high lenels of a structurally modified, activated form of pp60c-src. Nature 316:554–557.

Carreno S, Gouze ME, Schaak S, Emorine LJ, Maridonneau-Parini I. 2000. Lack of palmitoylation redirects $p59^{Hck}$ from the plasma membrane to $p61^{Hck}$-positive lysosomes. J Biol Chem 275:36223–36229.

Chang AH, O'Shaughnessy MV, Jirik FR. 2001. Hck SH3 domain-dependent abrogation of Nef-induced class I MHC down-regulation. Eur J Immunol 31:2382–2387.

Chitu V, Stanley ER. 2006. Colony-stimulating factor-1 in immunity and inflammation. Curr Opin Immunol 18:39–48.

David-Pfeuty T, Nouvian-Dooghe Y. 1990. Immunolocalization of the cellular src protein in interphase and mitotic NIH c-src overexpresser cells. J Cell Biol 111:3097–3116.
Deacon NJ, Tsykin A, Solomon A, Smith K, Ludford-Menting M, Hooker DJ, McPhee DA, Greenway AL, Ellett A, Chatfield C, Lawson VA, Crowe S, Maerz A, Sonza S, Learmont, Sullivan JS, Cunningham A, Dwyer D, Mills J. 1995. Genomic structure of an attenuated quasi species of HIV-1 from a blood transfusion and recipients. Science 270:988–991.
Drakesmith H, Chen N, Ledermann H, Screaton G, Townsend A, Xu XN. 2005. HIV-1 Nef down-regulates the hemochromatosis protein HFE, manipulating cellular iron homeostasis. Proc Natl Acad Sci USA 102:11017–11022.
Fackler OT, Baur AS. 2002. Live and let die: Nef functions beyond HIV replication. Immunity 16:493–497.
Fackler OT, Wolf D, Weber HO, Laffert B, D'Aloja P, Schuler-Thurner B, Geffin R, Saksela K, Geyer M, Peterlin BM, Schuler G, Baur AS. 2001. A natural variability in the proline-rich motif of Nef modulates HIV-1 replication in primary T cells. Curr Biol 11:1294–1299.
Greenberg ME, Iafrate AJ, Skowronski J. 1998. The SH3 domain-binding surface and an acidic motif in HIV-1 nef regulate trafficking of class I MHC complexes. EMBO J 17:2777–2789.
Haller C, Rauch S, Fackler OT. 2007. HIV-1 Nef employs two distinct mechanisms to modulate Lck subcellular localization and TCR induced actin remodeling. PLoS ONE 2:e1212.
Hamilton JA. 2008. Colony-stimulating factors in inflammation and autoimmunity. Nat Rev Immunol 8:533–544.
Hanna Z, Kay DG, Rebai N, Guimond A, Jothy S, Jolicoeur P. 1998. Nef harbors a major determinant of pathogenicity for and AIDS-like disease induced by HIV-1 in transgenic mice. Cell 95:163–175.
Hanna Z, Weng X, Kay DG, Poudrier J, Lowell C, Jolicoeur P. 2001. The pathogenicity of human immunodeficiency virus (HIV) type 1 Nef in CD4C/HIV transgenic mice is fabolished by mutation of its SH3-binding domain, and disease development is delayed in the absence of Hck. J Virol 75:9378–9392.
Hashimoto S, Hirose M, Hashimoto A, Morishige M, Yamada A, Hosaka H, Akagi K, Ogawa E, Oneyama C, Agatsuma T, Okada M, Kobayashi H, Wada H, Nakano H, Ikegami T, Nakagawa A, Sabe H. 2006. Targeting AMAP1 and cortactin binding bearing an atypical src homology 3/proline interface for prevention of breast cancer invasion and metastasis. Proc Natl Acad Sci USA 103:7036–7041.
Hiyoshi M, Suzu S, Yoshidomi Y, Hassan R, Harada H, Sakashita N, Akari H, Motoyoshi K, Okada S. 2008. Interaction between Hck and HIV-1 Nef negatively regulates cell surface expression of M-CSF receptor. Blood 111:243–250.
Hung CH, Thomas L, Ruby CE, Atkins KM, Morris NP, Knight ZA, Scholz I, Barklis E, Weinberg AD, Shokat KM, Thomas G. 2007. HIV-1 Nef assembles a Src family kinase-ZAP-70/Syk-PI3K cascade to down-regulate cell surface MHC-I. Cell Host Microbe 1:121–133.
Kaplan KB, Swedlow JR, Varmus HE, Morgan DO. 1992. Association of $p60^{c\text{-}src}$ with endosomal membranes in mammalian fibroblasts. J Cell Biol 118:321–333.
Karkkainen S, Hiipakka M, Wang JH, Kleino I, Vaha-Jaakkola M, Renkema GH, Kiss M, Wagner R, Saksela K. 2006. Identification of preferred protein interactions by phage-display of the human Src homology-3 proteome. EMBO Rep 7:186–191.
Kasahara K, Nakayama Y, Ikeda K, Fukushima Y, Matsuda D, Horimoto S, Yamaguchi N. 2004. Trafficking of Lyn through the Golgi caveolin involves the charged residues on αE and αI helices in the kinase domain. J Cell Biol 165:641–652.
Kestler HW III, Ringler DJ, Mori K, Panicali DL, Sehgal PK, Daniel MD, Desrosiers RC. 1991. Importance of the nef gene for maintenance of high virus loads and for development of AIDS. Cell 65:651–662.
Kirchhoff F, Greenough TC, Brettler DB, Sullivan JL, Desrosiers RC. 1995. Brief report: Absence of intact nef sequences in a long-term survivor with nonprogressive HIV-1 infection. N Engl J Med 332:228–232.
Korade-Mirnics Z, Corey SJ. 2000. Src kinase-mediated signaling in leukocytes. J Leukocyte Biol 68:603–613.
Lerner EC, Smithgall TE. 2002. SH3-dependent stimulation of Src-family kinase autophosphorylation without tail release from the SH2 domain in vivo. Nat Struct Biol 9:365–369.
Ley SC, Marsh M, Bebbington CR, Proudfoot K, Jordan P. 1994. Distinct intracellular localization of Lck and Fyn protein tyrosine kinases in human T lymphocytes. J Cell Biol 125:639–649.
Lowell CA. 2004. Src-family kinases: Rheostats of immune cell signaling. Mol Immunol 41:631–643.
Mangasarian A, Piguet V, Wang JK, Chen YL, Trono D. 1999. Nef-induced CD4 and major histocompatibility complex class I (MHC-I) down-regulation are governed by distinct determinants: N-terminal alpha helix and proline repeat of Nef selectively regulate MHC-I trafficking. J Virol 73:1964–1973.
Matsuda D, Nakayama Y, Horimoto S, Kuga T, Ikeda K, Kasahara K, Yamaguchi N. 2006. Involvement of Golgi-associated Lyn tyrosine kinase in the translocation of annexin II to the endoplasmic reticulum under oxidative stress. Exp Cell Res 312:1205–1217.
Mitina O, Warmuth M, Krause G, Hallek M, Obermeier A. 2007. Src family tyrosine kinases phosphorylate Flt3 on juxtamembrane tyrosines and interfere with receptor maturation in a kinase-dependent manner. Ann Hematol 86:777–785.
Moarefi I, LaFevre-Bernt M, Sicheri F, Huse M, Lee CH, Kuriyan J, Miller WT. 1997. Activation of the Src-family tyrosine kianse Hck by SH3 domain displacement. Nature 385:650–653.
Oneyama C, Agatsuma T, Kanda Y, Nakano H, Sharma SV, Nakano S, Narazaki F, Tatsuta K. 2003. Synthetic inhibitors of proline-rich ligand-mediated protein-protein interaction: Potent analogs of UCS15A. Chem Biol 10:443–451.
Paliwal P, Radha V, Swarup G. 2007. Regulation of p73 by Hck through kinase-dependent and independent mechanisms. BMC Mol Biol 8:45.
Peterlin BM, Trono D. 2003. Hide, shield and strike back: How HIV-infected cells avoid immune eradication. Nat Rev Immunol 3:97–107.
Priceputu E, Hanna Z, Hu C, Simard MC, Vincent P, Wildum S, Schindler M, Kirchhoff F, Jolicoeur P. 2007. Primary human immunodeficiency virus type 1 Nef alleles show major differences in pathogenicity in transgenic mice. J Virol 81:4677–4693.
Pulvirenti T, Giannotta M, Capestrano M, Capitani M, Pisanu A, Polishchuk RS, San Pietro E, Beznoussenko GV, Mironov AA, Turacchio G, Hsu VW, Sallese M, Luini A. 2008. A traffic-activated Golgi-based signaling circuit coordinates the secretory pathway. Nat Cell Biol 10:912–922.
Roeth JF, Collins KL. 2006. Human immunodeficiency virus type 1 Nef: Adapting to intracellular trafficking pathways. Mol Biol Rev 70:548–563.
Saksela K, Cheng G, Baltimore D. 1995. Proline-rich (PxxP) motifs in HIV-1 Nef bind to SH3 domains of a subset of Src kinases and are required for the enhanced growth of Nef^{+} viruses but not for down-regulation of CD4. EMBO J 14:484–491.
Schwartz O, Marechal V, Le Gall S, Lemonnier F, Heard JM. 1996. Endocytosis of major histocompatibility complex class I molecules is induced by the HIV-1 Nef protein. Nat Med 2:338–342.
Suzu S, Tanaka-Douzono M, Nomaguchi K, Yamada M, Hayasawa K, Kimura F, Motoyoshi K. 2000. $p56^{dok\text{-}2}$ as a cytokine-inducible inhibitor of cell proliferation and signal transduction. EMBO J 19:5114–5122.
Suzu S, Harada H, Matsumoto T, Okada S. 2005. HIV-1 Nef interferes with M-CSF receptor signaling through Hck activation and inhibits M-CSF bioactivities. Blood 105:3230–3237.
Trible RP, Emert-Sedlak L, Smithgall TE. 2006. HIV-1 Nef selecyively activates Src family kinases Hck, Lyn, and c-Src through SH3 domain interaction. J Biol Chem 281:27029–27038.
Ueno T, Motozono C, Dohki S, Mwimanzi P, Rauch S, Fackler OT, Oka S, Takiguchi M. 2008. CTL-mediated selective pressure influences dynamic evolution and pathogenetic functions of HIV-1 Nef. J Immunol 180:1107–1116.
van't Hof W, Resh MD, 1997. Rapid plasma membrane anchoring of newly synthesized p59fyn: Selective requirement for NH_2-terminal myristoylation and palmitoylation at cysteine-3. J Cell Biol 136:1023–1035.

HIV-1 Vif-mediated ubiquitination/degradation of APOBEC3G involves four critical lysine residues in its C-terminal domain

Yasumasa Iwatani[a,b,c,1], Denise S. B. Chan[d,e], Lin Liu[d], Hiroaki Yoshii[a], Junko Shibata[a], Naoki Yamamoto[c], Judith G. Levin[f], Angela M. Gronenborn[d], and Wataru Sugiura[a,b,c]

[a]Clinical Research Center, National Hospital Organization Nagoya Medical Center, Nagoya, Aichi 460-0001, Japan; [b]University of Nagoya Graduate School of Medicine, Nagoya, Aichi 466-8550, Japan; [c]AIDS Research Center, National Institute of Infectious Diseases, Tokyo 162-8640, Japan; [d]Department of Structural Biology, University of Pittsburgh Medical School, Pittsburgh, PA 15260; [e]Department of Chemistry, University of Hong Kong, Pokfulam Road, Hong Kong, China; and [f]Laboratory of Molecular Genetics, Eunice Kennedy Shriver National Institute of Child Health and Human Development, National Institutes of Health, Bethesda, MD 20892

Edited by John M. Coffin, Tufts University School of Medicine, Boston, MA, and approved September 24, 2009 (received for review June 16, 2009)

During coevolution with the host, HIV-1 developed the ability to hijack the cellular ubiquitin/proteasome degradation pathway to counteract the antiviral activity of APOBEC3G (A3G), a host cytidine deaminase that can block HIV-1 replication. Abrogation of A3G function involves the HIV-1 Vif protein, which binds A3G and serves as an adapter molecule to recruit A3G to a Cullin5-based E3 ubiquitin ligase complex. Structure-guided mutagenesis of A3G focused on the 14 most surface-exposed Lys residues allowed us to identify four Lys residues (Lys-297, 301, 303, and 334) that are required for Vif-mediated A3G ubiquitination and degradation. Substitution of Arg for these residues confers Vif resistance and restores A3G's antiviral activity in the presence of Vif. In our model, the critical four Lys residues cluster at the C terminus, opposite to the known N-terminal Vif-interaction region in the protein. Thus, spatial constraints imposed by the E3 ligase complex may be an important determinant in Vif-dependent A3G ubiquitination.

structure model | deaminase | antiviral

Human APOBEC3G (hA3G), is a host cytidine deaminase that has two homologous Zn cluster (H/C)XE(X)$_{23-28}$CXXC-containing domains [reviewed in (1, 2)]. Sheehy et al. (3) identified hA3G as the cellular factor that blocks HIV-1 replication in certain T cells (e.g., H9 or primary T-cell lymphocytes) in the absence of the viral protein Vif. Cellular expression of A3G results in its incorporation into *vif*-deficient HIV-1 particles, whereas the presence of A3G in wild-type (WT) virions is dramatically reduced by Vif-induced degradation via the ubiquitination-proteasome pathway before virion assembly and release (4–9). There is also evidence for other degradation-independent mechanisms (10, 11 and references therein).

In the absence of Vif, virion-encapsidated A3G causes extensive C-to-U mutations in synthesized minus-strand viral DNA and also physically blocks reverse transcription, rendering the virus noninfectious [(12–14) and reviewed in (11)]. Thus, given Vif's critical role in eliminating A3G function, it may be viewed as one of the most attractive pharmacologic targets for an anti-HIV drug aimed at restoring the activity of the intrinsic antiviral factor A3G in the context of HIV-1 infection. Indeed, such efforts have already begun. A recent report describes the small molecule inhibitor (RN-18) that increases cellular levels of A3G and incorporation of A3G into virions in a Vif-dependent manner (15).

Ubiquitination is catalyzed by a complex cascade system consisting of the ubiquitin (Ub)-activating (E1), Ub-conjugating (E2), and Ub-ligating (E3) enzymes (16, 17). Among these enzymes, the E3 class represents a diverse family of protein complexes, responsible for the selection of the target proteins. In particular, the Cullin-based E3 enzymes belong to the family of RING E3 Ub ligases that contain three main components: a Cullin (Cul1, 2, 3, 4a, 4b, 5, and 7), an adaptor, and a substrate receptor (18). In the Vif-A3G system, these proteins are Cul5, elongin B/C (EloB/C), and Vif, respectively. Cullin functions as a molecular scaffold on which the adaptor protein and receptor assemble to bring a specific substrate in close proximity to the E2 Ub-conjugating enzyme. The substrate receptor determines the specificity of the protein to be degraded and binds to Cullin through the adaptor protein. The E2-conjugating enzyme transfers multiple Ub molecules to the substrate, targeting it for degradation by the proteasome.

In general, the first Ub is typically conjugated to an ε-amino group of an internal Lys in the substrate (in this case, A3G). HIV-1 Vif, serving as the substrate receptor, facilitates ubiquitination of A3G by simultaneously binding to the Cul5-EloB/EloC-Rbx-E2 complex, thereby mimicking the function of cellular suppressor of cytokine signaling (SOCS) box proteins (9, 19–21). The SOCS box-like motif of Vif is highly conserved among primate lentiviruses and contains a BC box, as well as a Cullin box. The BC box motif creates a hydrophobic interface for binding to EloC. The Cullin box has a specific site for binding to Cul5, which involves an interaction between the highly conserved HCCH zinc-binding motif in Vif and the N-terminal domain (NTD) of Cul5 (22, 23).

Interestingly, it has been reported that Vif contains three sequence motifs for binding to A3G: $_{12}$QVDRMR$_{17}$; $_{40}$YRHHY$_{44}$; and $_{69}$YXXL$_{72}$ (24–26). The region in A3G responsible for binding to HIV-1 Vif was initially identified by comparative studies of the species specificity of A3G degradation by Vif. Thus, a single amino acid difference in hA3G, Asp at position 128 versus Lys in the A3G of African green monkeys (A3G$_{agm}$), determines species specificity by influencing Vif-A3G binding (27–30). Furthermore, extensive site-directed mutagenesis revealed that the $_{128}$DPD$_{130}$ motif of A3G, located near the first Zn cluster, is crucial for direct binding to HIV-1 Vif. It is of interest that this motif is just downstream of residues $_{124}$YYFW$_{127}$, which are involved in A3G's ability to bind nucleic acids (31).

Author contributions: Y.I., D.S.B.C., J.G.L., A.M.G., and W.S. designed research; Y.I., D.S.B.C., L.L., H.Y., and J.S. performed research; Y.I. contributed new reagents/analytic tools; Y.I., D.S.B.C., L.L., N.Y., J.G.L., A.M.G., and W.S. analyzed data; and Y.I., D.S.B,C., J.G.L., and A.M.G. wrote the paper.

The authors declare no conflict of interest.

This article is a PNAS Direct Submission.

Freely available online through the PNAS open access option.

[1]To whom correspondence should be addressed at: Clinical Research Center, National Hospital Organization Nagoya Medical Center, 4-1-1 San-no-maru, Naka-ku, Nagoya, Aichi 460-0001, Japan. E-mail: iwataniy@nnh.hosp.go.jp.

This article contains supporting information online at www.pnas.org/cgi/content/full/0906652106/DCSupplemental.